AD-A150 670   AN INVESTIGATION OF ELEVATED TEMPERATURE FATIGUE CRACK   1/2
           INITIATION IN 2 AND 1/4 CR-1 MO LOW ALLOY STEEL(U)
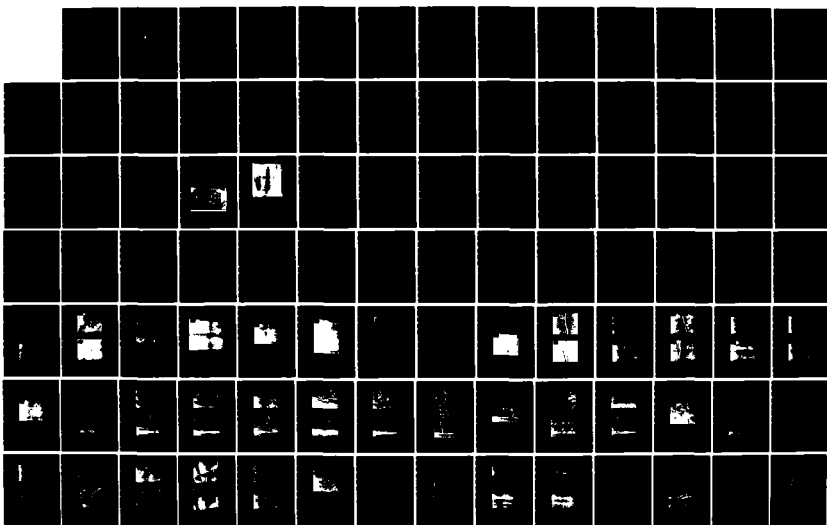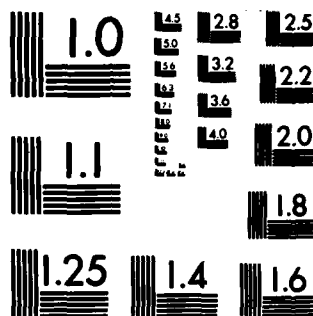   NAVAL POSTGRADUATE SCHOOL MONTEREY CA   O P KEIFER
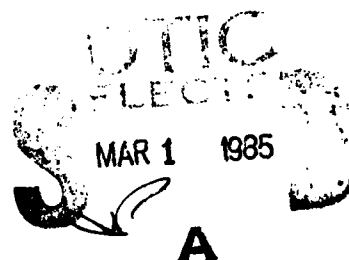UNCLASSIFIED   JUN 84   F/G 11/6   NL

MICROCOPY RESOLUTION TEST CHART
NATIONAL BUREAU OF STANDARDS-1963-A

AD-A150 670

NAVAL POSTGRADUATE SCHOOL
Monterey, California

MAR 1 1985

A

THESIS

AN INVESTIGATION OF ELEVATED TEMPERATURE
FATIGUE CRACK INITIATION IN
2¼ CR-1 MO LOW ALLOY STEEL

by

Orion P. Keifer

June 1984

Thesis Advisor: K. D. Challenger

85   02   13   018

REPORT DOCUMENTATION PAGE		READ INSTRUCTIONS BEFORE COMPLETING FORM
1. REPORT NUMBER	2. GOVT ACCESSION NO.	3. RECIPIENT'S CATALOG NUMBER
4. TITLE (and Subtitle) An Investigation of Elevated Temperature Fatigue Crack Initiation in 2¼ Cr-1 Mo Low Alloy Steel		5. TYPE OF REPORT & PERIOD COVERED Master's Thesis; June 1984
		6. PERFORMING ORG. REPORT NUMBER
7. AUTHOR(s) Orion P. Keifer		8. CONTRACT OR GRANT NUMBER(s)
9. PERFORMING ORGANIZATION NAME AND ADDRESS Naval Postgraduate School Monterey, California 93943		10. PROGRAM ELEMENT, PROJECT, TASK AREA & WORK UNIT NUMBERS
11. CONTROLLING OFFICE NAME AND ADDRESS Naval Postgraduate School Monterey, California 93943		12. REPORT DATE June 1984
		13. NUMBER OF PAGES 111
14. MONITORING AGENCY NAME & ADDRESS(if different from Controlling Office)		15. SECURITY CLASS. (of this report) Unclassified
		15a. DECLASSIFICATION/DOWNGRADING SCHEDULE

16. DISTRIBUTION STATEMENT (of this Report)

Approved for public release; distribution unlimited.

17. DISTRIBUTION STATEMENT (of the abstract entered in Block 20, if different from Report)

18. SUPPLEMENTARY NOTES

19. KEY WORDS (Continue on reverse side if necessary and identify by block number)

Fatigue, oxide cracking, 2¼ Cr - 1 Mo Steel

20. ABSTRACT (Continue on reverse side if necessary and identify by block number)

Environmental effects in elevated temperature fatigue have been extensively studied and reported in the literature for 2¼ Cr-1 Mo steel. The results of cycles to failure (lumped initiation and propagation life) verses strain range have shown drastic reductions in fatigue life with a dwell period at compressive strains in each loading cycle. This thesis has separately examined the crack initiation and propagation stages for several specimens tested in air at 538 °C without dwell and

DD FORM 1473 EDITION OF 1 NOV 65 IS OBSOLETE
1 JAN 73
S/N 0102-LF-014-6601

a single specimen with a five minute compressive dwell. With dwell, the crack initiation stage was severely reduced (by a factor greater than eleven) relative to testing without dwell. The results clearly indicate that oxide cracking is a precursor to crack initiation in the substrate. It is concluded that the fatigue life of this alloy must be estimated based on the crack propagation characteristics alone, since crack initiation can be expected very early (i.e. first few cycles) for any practical environment. Originator

Supplied Keywords include:

ii

An Investigation of Elevated Temperature
Fatigue Crack Initiation in
2 1/4 Cr-1 Mo Low Alloy Steel

by

Orion P. Keifer
Lieutenant Commander, United States Navy
B.S.M.E., United States Naval Academy, 1973

Submitted in partial fulfillment of the
requirements for the degree of

MASTER OF SCIENCE IN MECHANICAL ENGINEERING

from the

NAVAL POSTGRADUATE SCHOOL
June 1984

Author: _____

Approved by: _____
                                   Thesis Advisor

_____
                                   Second Reader

_____
Chairman, Department of Mechanical Engineering

_____
                   Dean of Science and Engineering

3

ABSTRACT

Environmental effects in elevated temperature fatigue have been extensively studied and reported in the literature for 2 1/4 Cr-1 Mo steel. The results of cycles to failure (lumped initiation and propagation life) verses strain range have shown drastic reductions in fatigue life with a dwell period at compressive strains in each loading cycle. This thesis has separately examined the crack initiation and propagation stages for several specimens tested in air at 538 °C without dwell and a single specimen with a five minute compressive dwell. With dwell, the crack initiation stage was severely reduced (by a factor greater than eleven) relative to testing without dwell. The results clearly indicate that oxide cracking is a precursor to crack initiation in the substrate. It is concluded that the fatigue life of this alloy must be estimated based on the crack propagation characteristics alone, since crack initiation can be expected very early (i.e. first few cycles) for any practical environment.

4

TABLE OF CONTENTS

LIST OF TABLES

LIST OF FIGURES

9

ACKNOWLEGEMENTS

I. INTRODUCTION

Annealed 2.25% Cr 1% Mo steel is a ferritic, low alloy steel that has been used extensively for elevated temperature applications in the power generating industry for over thirty years. The alloy is readily available, easily fabricated, has good elevated temperature strength and creep resistance, and extensive data is available from operational employment. More recently, the alloy has been used in the nuclear industry and was selected for steam generator application in the Clinch River Liquid Metal Cooled Fast Breeder Reactor (CRLMCFBR). Because the ASME Pressure Vessel Code requires that accurate predictions be made for elevated temperature fatigue life of materials used in nuclear applications, extensive research was organized and coordinated by the Oak Ridge National Laboratory (ORNL), in the area of fatigue and creep for this alloy in support of the CRLMCFBR. Although the CRLMCFBR project has been abandoned, there is continued interest in this alloy for conventional and future nuclear applications.

In this research, crack initiation and propagation during the course of fatigue testing has been examined and results compared with the fatigue life data generated by the ORNL experimental program. The purpose of this thesis is to better understand the first two phases of fatigue, namely crack initiation and crack propagation, in order to better predict expected life of components made of this alloy and subjected to fatigue loading. Additionally, this thesis examines the effect of the oxide layer that forms at elevated temperatures in order to establish its importance in crack initiation.

12

The balance of this thesis will present the background
of the fatigue characteristics of this alloy at elevated
temperatures, the experimental procedures used, the results
and conclusions of this study, and the recommendations for
further study.

II. BACKGROUND

A. GENERAL

Elevated temperature components in power generation plants must withstand local cyclic stresses and strains beyond yield. Normal plant operations will produce temperature gradients of a cyclic nature during startups, shutdowns and changes in power level. Abnormal conditions, caused by equipment failure, various casualty conditions, and operator error can cause even more severe temperature transients. These thermal cycles, and associated temperature gradients, subject elevated temperature components to thermal stress-strain cycles which may involve plastic flow. Areas of localized tension and compression are developed, with variable hold times at extreme strain levels, which can result in creep interspersed with fatigue cycling. In addition, these components are exposed to various environments, such as steam, combustion product gases, liquid sodium, water, and air.

The fatigue lives of these components depend on many factors such as, temperature, creep rate, stress-strain magnitudes and rates, environmental effects such as oxidation, decarburization and depletion of alloys, initial microstructure and microstructural changes, as well as time. Considerable fatigue life data has been generated on this and closely related alloys in various environments, with various initial microstructures, and different fatigue loading wave forms in order to determine the most significant interactions. The goal, of course, is to develop a predictive model for use of designers.

14

There has been considerable debate over the past several
years as to the relative importance of the creep-fatigue and
the environmental-fatigue interactions in fatigue life of
this alloy. Although decreased fatigue life due to environ-
mental effects has long been known, much of the earlier
research attributed the decrease in fatigue life resulting
from dwell periods to the creep-fatigue interaction. This
is a natural consequence of ASME design method for analyzing
the problem by ignoring any environmental effects, with
satisfactory predictive fatigue models produced for austen-
itic steels. More recently, other researchers have
concluded that the creep-fatigue interaction in ferritic
alloys, such as 2 1/4 Cr-1 Mo steel, is minor and can be
ignored, and the dominant effect is environmental [Ref. 1].

Conclusive evidence exist that in 2 1/4 Cr - 1 Mo steel
that the dominant effect is due to environmental-fatigue
interaction. A brief summary is given here with more
complete discussion in later sections. First, less
oxidizing environments increase the cyclic lifetime espe-
cially at low (<1%) total strain ranges. This has been
shown in impure Helium [Ref. 2], vacuum [Ref. 3] and liquid
sodium [Ref. 4]. Second, Haigh [Ref. 5] reported that crack
propagation in vacuum for a closely related alloy (1
Cr-Mo-V) at 500 °C was up to 100 times slower than in air
for the same test temperature, and was about the same as
tests conducted in air at room temperature, where oxidation
is minimal. Third, tests performed with dwell periods at
zero stress in order to minimize creep damage, yet allow
oxidation damage to occur [Ref. 6, 7], showed that the
fatigue life of the specimen with the dwell after the
compressive half cycle and the dwell after the tensile half
cycle had about the same life as those with the the dwell at
maximum compressive strain and maximum tensile strain
respectively. This showed that creep had no effect. Other

tests in vacuum [Ref. 8] and helium [Ref. 9] show that with minimal oxidation, dwell periods have a relatively minor effect on fatigue life, compared to specimens that are continuously cycled.

Each of the above tests indicate that the creep-fatigue interaction can be neglected, a conclusion reached by Challenger [Ref. 1]. Therefore the remainder of the background will be devoted to the environmental-fatigue interactions.

B. OXIDATION CHARACTERISTICS

1. Oxide Growth

In general, the extent of oxidation in air for ferrous alloys like 2 1/4 Cr - 1 Mo Steel can be expressed in terms of h, the oxide thickness, which varies parabolically with time and follows an Arrhenius temperature dependence. Challenger [Ref. 7] empirically determined the constants for this relationship during fatigue cycling, using weight reduction data from the Nuclear Systems Material Handbook [Ref. 10] and from oxide thickness measurements by Langdon [Ref. 11]. Equation 2.1 is the resultant formula:

$$h = 1.26 \times 10^{-3} \exp[-12210/RT] \, t^{1/2} \qquad \text{(eqn 2.1)}$$

where h is the oxide thickness in meters, t is the elapsed time in hours, T is the absolute temperature in $^\circ$K, and R is the gas constant. This expression was found to agree favorably with results obtained from a fatigue specimen tested at 538 $^\circ$C for 160 hours.

The oxide layer has been found to develop a duplex form with two discernable layers [Ref. 12, 13]. The inner

16

layer contains about the same concentration of Cr and Mo as the base metal, while the outer layer is devoid of these alloying elements and is instead pure magnetite. The interface between these layers correspond well with the initial surface of the metal and thus oxide penetration can be measured directly.

The oxidation growth rate depends on several variables. Armitt et al [Ref. 13] reported that the oxidation rate depends on grain size and initial surface finish. In addition, Challenger [Ref. 7] found that for 2 1/4 Cr - 1 Mo that the oxidation rate of cyclically deformed material is faster than for free oxidation. Similar results were reported by Skelton [Ref. 14] for 1 Cr-Mo-V steel, and Armitt et al [Ref. 13] for 9 Cr-Mo.

2. Oxide Characteristics

a. Thermal Expansion Coefficient

Gordon [Ref. 15] calculated the differential thermal expansion coefficients for iron and its oxides as a function of temperature using X-ray diffraction techniques to measure the changes in lattice parameter. McElroy [Ref. 16] compiled thermal expansion data for several low alloy steels, as well as for iron. The data for iron had similar values in the above two references, indicating that the two methods of measurement produce comparable results. McElroy calculated the differential thermal expansion coefficient for the material of nominal 2 1/4 Cr - 1 Mo Steel composition, and stated a coefficient uncertainty of 4%. Table I is a summary of the thermal expansion data.

b. Modulus of Elasticity

Many measurements of the modulus of elasticity for oxide films have been made [Ref. 13] but the results are

17

TABLE I

Thermal Expansion Coefficients

$(°C^{-1} \times 10^6)$

Temp	Iron[1]	Magnetite[1]	Haematite[1]	2 1/4 Cr-1 Mo[2]
25 °C	13.22	10.41	10.96	11.497[3]
200 °C	13.63[3]	12.68	10.45	13.505
300 °C	14.81	13.97	11.82	14.345
400 °C	15.35	15.26	12.15	14.957
500 °C	15.99[3]	16.54	12.45	15.341

[1] Reference 15
[2] Reference 16
[3] Denotes that the value was linearly interpolated.

rather inconsistent. For example, Field [Ref. 17] measured the modulus of elasticity for magnetite on an iron substrate at 140-260 GPa using a simple cantilever specimen. Metcalfe [Ref. 18] measured the modulus of elasticity of a spalled magnetite - 20% haematite oxide scale formed in steam on an austenitic specimen. His results were 61 GPa using a three point bend method, and 84 GPa using an acoustic method. Additionally, Metcalfe [Ref. 18] measured the modulus of elasticity of the inner layer spinel of the duplex oxide film and reported a value of 25 GPa using the three point bending method and 32 GPa using the acoustic method. Exact values are uncertain, but the difference in the modulus of elasticity in the duplex oxide formation is conclusive.

c. Fracture Strain

Armitt, et al [Ref. 13] showed that the critical strain to crack an oxide follows equation 2.2,

$$\epsilon_c = [0.5\gamma/EC]^{1/2} \qquad \text{(eqn 2.2)}$$

where $\hat{\gamma}$ is the fracture surface energy, $\underline{E}$ is the modulus of elasticity, and $\underline{C}$ is the depth of the initiation flaw. Challenger [Ref. 7] has further assumed that the initiating crack size is proportional to the thickness of the oxide layer. He was able to empirically determine the constant using hour glass specimen data. The resultant analysis predicts the fracture strain as a function of oxide thickness according to:

$$\epsilon_c = [3.5 \times 10^{-11}/h]^{1/2} \qquad \text{(eqn 2.3)}$$

where $\underline{h}$ is in meters. Eqn 2.1 can be used to determine the critical thickness for a given strain, then Eqn 2.3 can be used to predict the time to reach this critical thickness. Therefore, it is possible to predict when oxide layer cracking will occur in a controlled test [Ref. 7].

C. WAVEFORM EFFECTS

Many studies have incorporated dwell periods on each cycle. From creep-fatigue interaction, one would expect dwell periods at maximum tensile strain would be more damaging than dwell periods at maximum compressive strain. This is found to hold true when this alloy is tested in a vacuum or inert environments, but the effects are relatively minor. In air or other oxidizing environments, however, compressive strain dwell periods severly shorten the fatigue life as compared to either tensile strain dwell periods or continuous cycling.

Challenger [Ref. 6] and Teranishi [Ref. 19] showed that the oxide will crack along a direction perpendicular to the maximum tensile stress. With a dwell period at maximum compressive strain (or zero stress dwell following the

19

compressive half cycle), the sample spends most of the time
in a compressive state and the oxide which forms during this
dwell period has a "stress free" state while the substrate
material is in compression. When the cycling is resumed,
the strain range imposed on the oxide layer corresponds to
the total strain range of the cycle and is entirely tensile
for the oxide layer, with maximum stress in the longitudinal
direction. Thus, cracks will form circumferentially around
the specimen.

In contrast, when the dwell period is at the maximum
tensile strain, (or at the zero stress condition following
the tensile half cycle), the "stress free " state in the
oxide will develop while the substrate has a tensile strain.
When cycling is resumed, the maximum tension in the oxide
will be in the circumferential direction and the strain
will be numerically equal to the total strain times
Poisson's ratio. Therefore, the critical strain to crack
the oxide will be reached only at a thicker oxide layer,
furthermore the cracks will be in the axial direction,
making it less likely to to become a fatigue crack initi-
ator. In any event, the oxide layer tends to spall off,
thereby minimizes crack initiation caused by oxide cracking.

The metal surface under the oxide layer is very
different as well, depending on whether dwell occurs in
tension or compression. With dwell at maximum compressive
strain, the surface has circumferential grooves, presumably
where the oxide cracks previously existed [Ref. 6]. With
tensile strain dwells, the surface is somewhat rougher than
the original specimen surface, but no grooves are present.

The data also indicates that the cirumferential oxide
cracks promote accelerated corrosion fingers in the
substrate which crack, thereby creating a stress concen-
trator which surve as a fatigue crack initiation site. This
explains why compressive hold periods are more damaging than
tensile holds in an oxidizing environment.

20

C. CRACK GROWTH

   1. Crack Size Effects

        Short cracks grow in a different manner than long
cracks in a given material. Taylor [Ref. 20] has shown that
for most metals, including ferrous alloys, cracks of depth
less than a critical value grow faster than predicted by
Linear Elastic Fracture Mechanics (LEFM). At crack depths
greater than the critical value, LEFM is valid. He also
concluded that the critical depth is highly dependent on the
microstructure. In particular, cracks of depths less than
one grain diameter show particularly rapid growth. Taylor
concluded that since LEFM assumes a homogeneous continuum
(closely approximated at greater crack depths), it cannot be
expected to be valid for short cracks. It is not surprising
that short cracks grow more rapidly than predicted by LEFM,
since smooth surfaces will crack in fatigue if the cyclic
stress is above the endurance limit, even though the stress
intensity factor for a smooth surface is zero.
        Skelton [Ref. 21] has also studied this phenomenon
in 0.5 Cr-Mo-V steel and concluded that LEFM hold for crack
lengths greater than about 0.2 mm (approximately 4 grain
diameters). He also showed that the crack growth rate was
greater for crack lengths less than this critical value.

   2. Oxidation Effects

        Skelton and Challenger [Ref. 22] have reported that
crack growth per cycle is greater in air than in vacuum,
except at very low total strains, and large crack depths.
Two explanations were offered. First, at larger strain
ranges in vacuum, the crack tip can reweld due to the
compressive portion of the cycle. For example in a single
test in vacuum with a compressive hold [Ref. 22], crack
growth ceased, suggesting rewelding at the crack tip.

21

Second, when testing in air, enhanced oxidation occurs
during the opening of the crack on the tensile half cycle.
This results in a wedging effect which promotes crack
growth. At low strain ranges or with long cracks, the oxide
layer on the two surfaces impinge on each other, effectively
sealing out the oxygen, a conclusion reach by both
Challenger [Ref. 1] and Skelton [Ref. 21]. Fatigue tests
conducted in air with a 1/2 hour hold time did not increase
crack growth rates over those measured in continuously
cycled specimens. The conclusion reached by Challenger
[Ref. 1] is that the oxidation effect must saturate very
quickly.

Challenger [Ref. 1] noted that the oxidation effect
decreases as crack growth rate increases and is negligible
at growth rates greater than $2x10^{-3}$ mm/cycle.

E. CRACK INITIATION PREDICTION

Mayia [Ref. 23] conducted extensive research on crack
initiation in 304 Stainless Steel (SS) at 593 °C, using a
sawtooth waveform at a strain rate of 0.004 sec^{-1}. He used
a replication technique to determine the number of cycles to
crack initiation (Nn), and then cycled the specimen to
failure to determine the number of cycles to failure (Nf).
His data was presented on a graph of Nn/Nf versus total
strain range. Challenger [Ref. 7] noted that 2 1/4 Cr - 1
Mo steel tested at elevated temperatures had similar slip
characteristics and fatigue strength as 304 SS.
Additionally, the portions of the total strain range which
are plastic are similar for 304 SS at 593 °C and 2 1/4 Cr -
1 Mo Steel when tested at 482 °C. He therefore used Mayia's
data to construct a plot of Nn/Nf verses total strain range
for 2 1/4 Cr - 1 Mo steel at 482 °C. In addition, extrapo-
lations of the curve were made for temperatures of 427 °C,

22
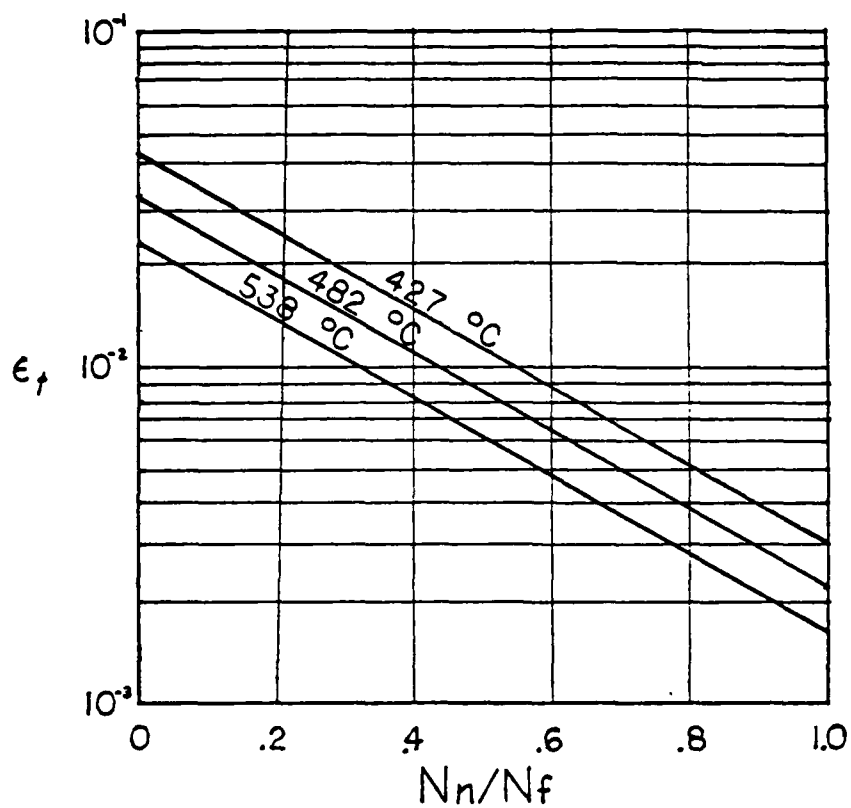
Figure 2.1   Nn/Nf vs. total strain range.

and 538 °C.   The resultant curves are shown on Figure 2.1.
This gives a basis for comparison for the results of this
thesis.

III. EXPERIMENTAL

A. GENERAL

A 10,000 Kg (22 KIP) MTS Electrohydraulic testing system, in conjunction with a Cycle-Dyne induction heater was used to conduct fatigue tests on specimens at elevated temperatures (538 °C). The specimens were uniaxially loaded at a strain rate of 4×10^{-3} sec^{-1} and were subjected to equal strains in tension and compression. Periodically, cycling was interrupted and the specimen was examined with a Scanning Electron Mircscope to monitor crack initiation and crack growth. The thrust of this work was to obtain the number of cycles to crack initiation, and also the fatigue life for total strain ranges between 0.3% and 1.0%.

B. APPARATUS

1. Equipment

Specific equipment used was as follows

    a. MTS Model 810 Electrohydraulic Testing System

1) MTS Model 312.21 Load Frame
2) MTS Model 661.21A-03 Load Cell
3) MTS Model 410 Function Generator
4) MTS Model 417 Counter Panel
5) MTS Model 4456 Controller with modules
6) MTS Model 506.01 Hydraulic Power Supply
7) Hewlett Packard 7045A X-Y Recorder

b. Heater

   1) Cycle-Dyne Model A-30 Induction Heater
   2) MTS Model 632.50B-01 High Temperature
      Extensometer
   3) MTS Type B2506-2 Knife Edge Quartz Extension
      Rods
   4) Research Model 63911 Temperature Control Panel
   4) Newport Model 267E-KC1 Digital Pyrometer
   5) User designed Induction Coil

c. Scanning Electron Microscopy

   1) Cambridge S4-10 Scanning Electron Microscope
      (SEM)
   2) User modified S-100 SEM Stage

2. Induction Coil Development

The induction coil configuration is critical for the control of the temperature along the specimen gage length. Direct monitoring of the gage length is impossible during actual testing, since the spot welding of the thermocouples to the gage length would result in a stress concentrater, and hence premature crack initiation. Therefore, indication of the gage length temperature by necessity must be derived by monitoring thermal couples welded outside the gage length on the specimen fillets, and with associated calibration data.

Ellison [Ref. 24] evaluated numerous coil configurations using an instrumented specimen with seven thermocouple monitoring points, as shown in Figure 3.1. The variables for the coil design were the number of turns and the spacing, size, and shape of the turns. Additional physical constraints on the coil design include the distance between the grips, allowance for the extensometer rods, space

25
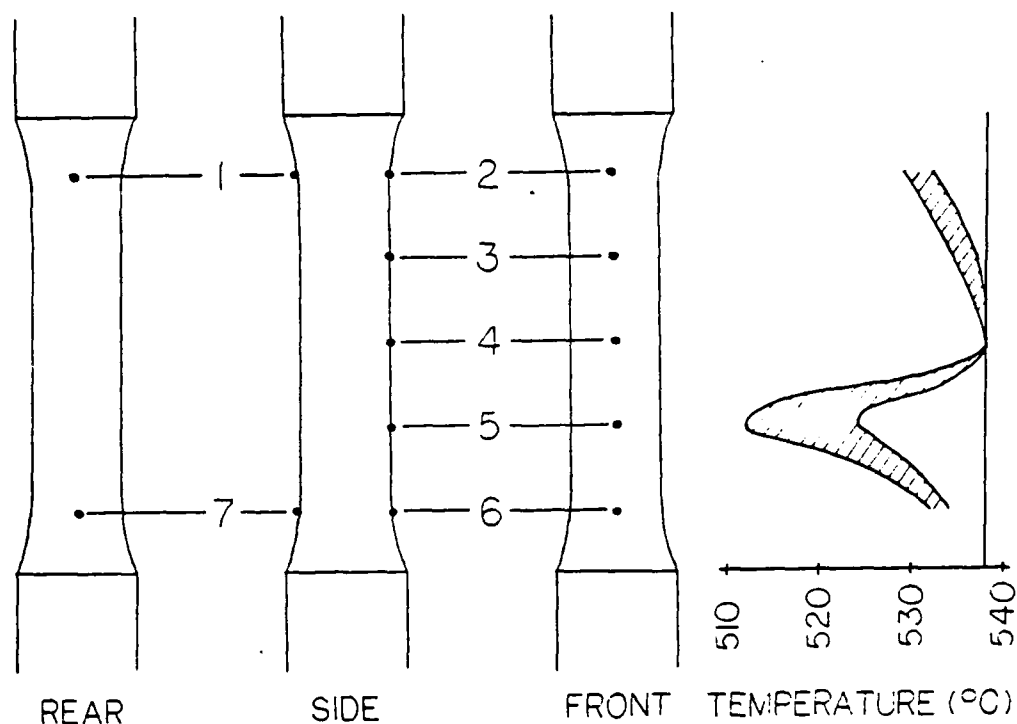
Figure 3.1   Instrumented Test Specimen.

necessary to insert and remove instrumented specimens, and
adequate allowance for the movement of the specimen during
cycling. Ellison found that the temperature profile was
very sensitive to all of the variables, and to the radial
and axial position of the coil with respect to the specimen.
Too many turns produced interferance with sensor signals,
too few turns caused steeper axial temperature gradients.
Incomplete turns caused large radial temperature gradients.
The optimum coil configuration was found to have two
complete turns top and bottom, separated slightly more on
the top, as shown in Figure 3.2.   It was hypothesised
[Ref. 24] that this was a result of the greater power
required to maintain temperature on the lower portion of the
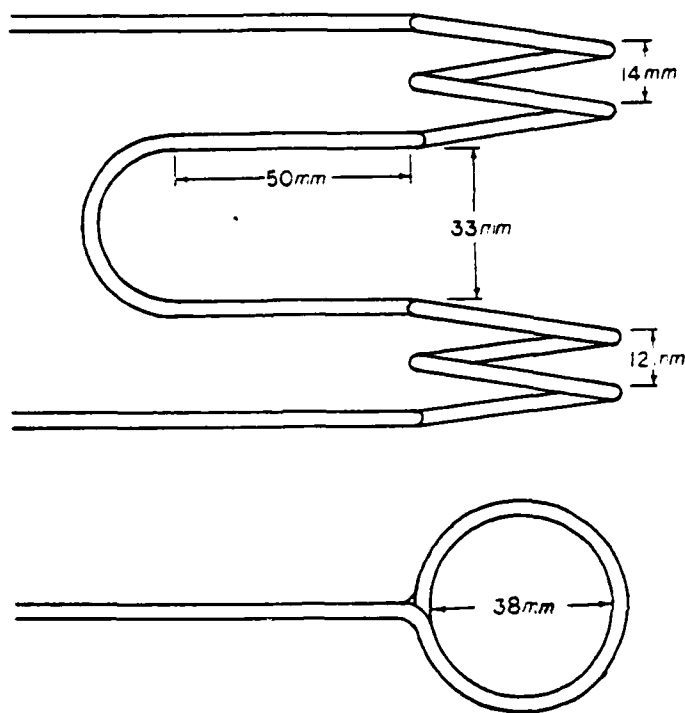
Figure 3.2   Optimum Coil Design.

sample due to greater conductive heat losses. Closer
spacing of the turns reduced the magnetic leakage and
increased the temperature. Figure 3.1 shows the temperature
profile obtained, with a diagram of the instrumented spec-
imen for reference. The band of temperatures represents the
result of slight changes of radial and axial position of the
coil with respect to the specimen, while holding thermo-
couple #4 at 538 ⁰C.

The actual temperature of the specimen gage sections
depend on several other variables. During initial setup
under static conditions, the set point temperature (top
thermocouple) could easily be adjusted with the temperature
controller to deviate less than 1 ⁰C from the calibration

27

setting. The monitoring temperature (bottom thermocouple) could normally be adjusted by moving the coil with respect to the specimen to obtain a deviation from calibration data of 1 °C or less. During cycling, the specimen moved axially inside the stationary coil due to the compliance of the MTS system. The temperature controller could maintain the setpoint temperature to within one degree, however the monitoring temperature frequently changed by as much as two degrees. The monitoring temperature tended to fluctuate with the cyclic motion of the specimen.

The thermocouple wires were spot welded separately to the specimen, with the two wires parallel. Ellison [Ref. 24] found that the spacing between the two wires was critical, and wide spacing introduced errors in the temperature readings. Great care was taken to minimize this error by welding the thermocouple wires as close together as possible.

3. Scanning Electron Microscope Stage Development

The Cambridge S4-10 stage normally has a maximum specimen size of approximatly one inch (25 mm) diameter and one half inch (13 mm) height. In order to accommodate the entire six inch (15.25 cm) tensile specimen, a Cambridge S100 stage was extensively modified. All internal parts were removed, leaving the feed-through flange with the associated five feed-through connections (two half-inch linear, one one-inch linear, and two rotational), and the base plate. New internal parts were designed by the author and manufactured by the Mechanical Engineering Machine Shop. The two rotational feed-throughs were used to produce longitudinal motion, through a lead screw, and rotational motion with gearing salvaged from the stage's original internal parts. One half-inch feed-through was used to provide transverse motion via a cam mechanism. The other feed-through

connections were not used.   This arrangement allowed two
inches (5 cm) of longitudinal motion, full rotational motion
about the longitudinal axis of the specimen,   and one half
inch (13 mm) transverse motion, suffient to view the entire
gage length without removing the specimen.   Due to the
length of the stage with the specimen inserted and the
internal placement of the detectors in the Cambridge SEM,
the stage was by necessity designed to be inserted in to the
left access port verses the normal front port.   This
required the electrical connections to be made prior to
insertion of the stage and the connector is no longer an
integral part of the stage.   Figure 3.3 shows the stage as
modified and Figure 3.4 shows the SEM with the stage
inserted.
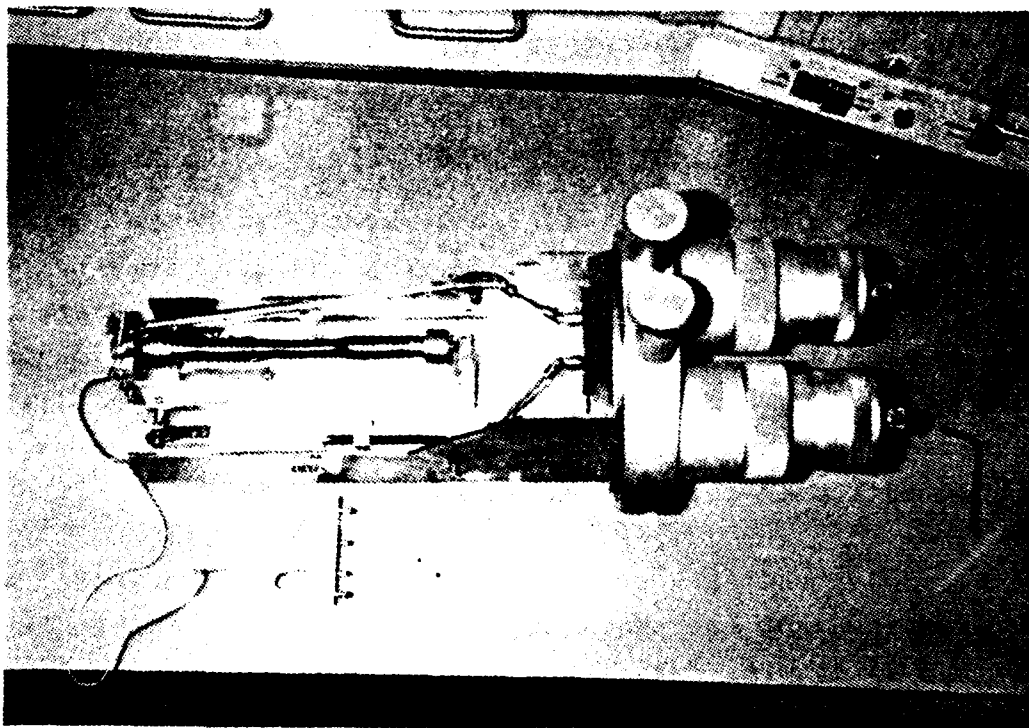
Figure 3.3   Modified Scanning Electron Microscope Stage.
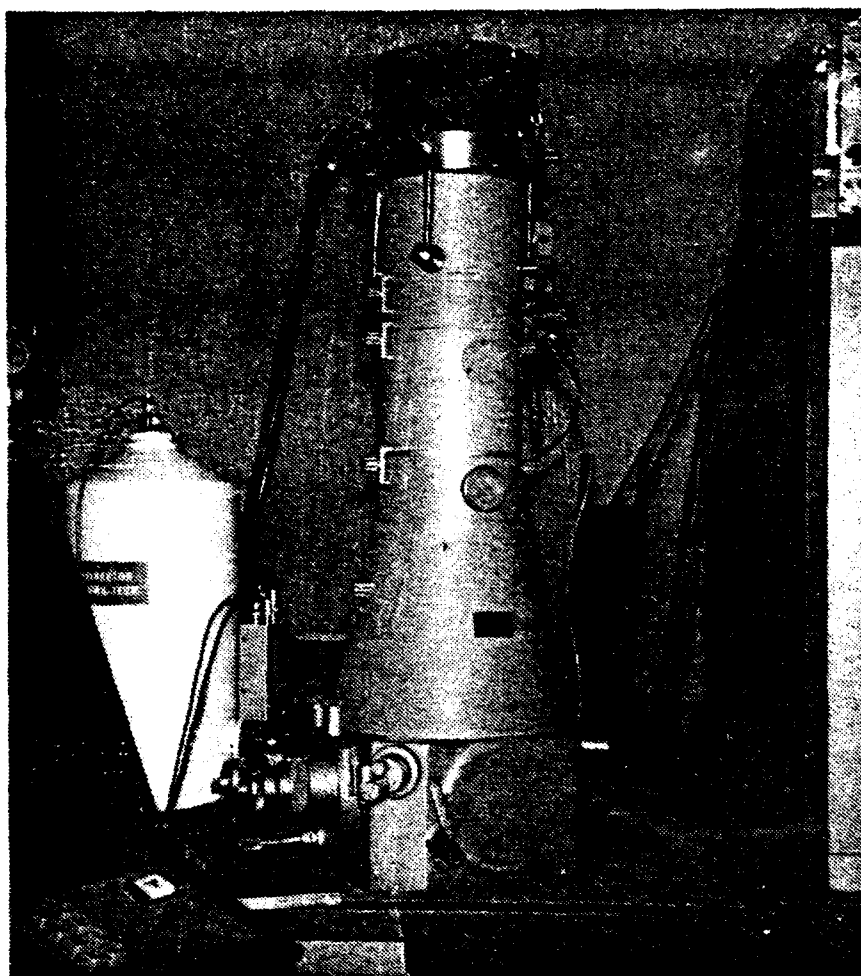
Figure 3.4   Cambridge S4 SEM with Modified Stage Inserted.

4.   MTS Electronic Control

A brief discussion of the MTS electronic controls is
useful in understanding the test procedure used in this
work.

a.   MTS Controller

Three parameters are sensed by the controller;
load, strain and stroke.   These signals are electronically
processed to give a full range signal of ±10 volts.   A
summary of the sensing parameters is contained in Table II.

30

```
                        TABLE II
                 MTS Controller Parameters

                                              Digital
    Parameter    Sensor        100% Range     Readout
    Load         Load Cell     ±20 kips       volts, lbs
    Strain       Extensometer  ±0.02 inches   volts, inches
    Stroke       Internal LVDT ±5 inches      volts, inches
```

Note that the sensor length of the extensometer
is one inch (2.54 cm), therefore extension and engineering
strain are numerically equivalent.

Each of these parameters has an individual
control module in the controller. These modules have a
potentiometer which allows for electronically nulling the
parameter. There is also a selector switch, which allows
changing the range scale to correspond to 100%, 50%, 20% or
10% of the total range to the ±10 volt output signal.

Any of these three parameters can be selected
for control. For these experiments, stroke control was used
while inserting or removing the sample, load control was
used during heatup and cooldown, and strain control was used
during the fatigue cycling. A setpoint potentiometer is
provided on the controller to adjust the static value of the
controlling parameter and to provide a reference voltage on
which the function generator signal is based.

The function generator generates a voltage
signal up to ± 10 volts, with various output functions
available such as sine, haver sine, ramp, and saw tooth, and
with various periods, slopes, and hold times. The various
possibilities are listed in Reference 25.

When a test is started, the controller adds the function generator signal to the setpoint signal and compares the sum to the controlling parameter signal. Hydraulic pressure is ported to the hydraulic actuator to force the error to zero.

b. Protection Devices

The MTS system has several protection devices, each of which has a positive peak setting and a negative peak setting, and an enable-disable switch. These devices include overload, over strain, excessive stroke, underpeak, and temperature deviation between the controlling thermocouple and the setpoint value on the temperature controller. When an interlock is enabled and it trips, the hydraulic power supply and induction heater is also tripped. The controller ports the residual hydraulic pressure to reduce the controlling parameter to zero, and as the pressure dies away, the load drops to near zero. The specimen cools at a very rapid rate due to natural convective losses.

C. TEST PROCEDURES

1. Specimen preparation

Specimens used for this testing were taken from a one inch (2.54 cm) diameter rod of 2.25% Cr-1% Mo steel, Heat Number 56447, provided by Oak Ridge National Laboritory (ORNL), and produced by Vacuum Arc Remelting (VAR) technique. Chemical analysis of representative material appears in Table III.

The rod was cut into sections, six and one half inches (16.5 cm) in length and these were heat treated as follows; Austenitize at 927 ±14 °C for one hour, cool to 704 ±14 °C at a maximum cooling rate of 83 °C per hour, hold for two hours, and then cool to room temperature at a rate not to exceed 6 °C per minute.

32

TABLE III

Chemical Composition of 2.25% Cr-1% Mo Steel

Heat Number 56447

Content Weight Percent

C	Mn	Si	Cr	Mo	Ni	S	P
0.098	0.53	0.22	2.20	1.03	0.24	0.005	0.059

Specimens were then machined and polished to provide a uniform gage length of 1.250 inches (31.8 mm) and a diameter of 0.375 inches (9.5 mm). Figure 3.5 provides a detailed drawing of the specimen with pertinent machining procedures. After machining, the specimens were cleaned locally using acetone and cotton swabs and rinsed with ethanol.

ANSI type K thermocouple wires were prepared by mechanically flattening the bare wires and spot welding them to the specimen gage fillets using a Unitec Model 1065 spot welder. Two thermocouples were attached, one on each fillet of the gage length, with the same radial orientation. These positions correspond to points #2 and #6 on the coil calibration specimen, shown in Figure 3.1. The thermocouple wire was held rigidly in place (to prevent breakage as the specimen was repeatedly inserted and removed) by bands of nickel foil spot welded over the insulated thermocouple wire. These bands were located between the gage portion and the button head. In addition, an insulator was inserted since the thermocouple wire insulation tended to become brittle at the elevated temperatures during testing.

The specimen was cleaned and swabbed with acetone and rinsed with ethanol, and the thermocouple and adjacent

33

NOTES:

1. REMOVE ALL BURRS AND SHARP EDGES.
2. SURFACE ROUGHNESS ∇ UNLESS OTHERWISE SPECIFIED.
3. SPECIMEN TO BE IDENTIFIED AT ALL TIMES DURING FABRICATION WITH MATERIAL HEAT NO. PLATE NO. HEAT TREATMENT AND SPECIMEN NO. BY DIE MARKING OR MASKING TAPE AND LABELED ENVELOPES.
4. MARK WITH APPLICABLE SPECIMEN NUMBER ON BOTH ENDS (SAME NUMBER AS BLOCK) ENGRAVE, DO NOT STAMP. VIBRATING TYPE ENGRAVING TOOL IS PERMISSIBLE.
5. FINAL MACHINING OF THE REDUCED SECTION AREA OF THE SPECIMEN SHALL BE AS FOLLOWS:
   A. ROUGH MACHINING SHALL LEAVE 0.010 in. STOCK ON THE RADIUS OVER THE FINAL DIMENSION.
   B. USING A GRINDING WHEEL WITH ITS SHAFT AT 90° TO THE SPECIMEN LONGITUDINAL AXIS GRIND WET.
   C. REMOVE 0.0002 in. STOCK MATERIAL EACH PASS WHILE ROTATING THE SPECIMEN AT 325 rpm ABOUT ITS LONGITUDINAL AXIS, SIMULTANEOUSLY TRANSLATING THE SPECIMEN BACK AND FORTH UNDER THE GRINDING WHEEL, PARALLEL TO THE GRINDING WHEEL SHAFT AXIS.
   D. BUFF TO 8-11 MICROINCH FINISH BY POLISHING IN A MANNER PARALLEL TO THE SPECIMEN LONGITUDINAL AXIS.
   E. POLISH REDUCED AREA LONGITUDINALLY TO REMOVE ALL CIRCUMFERENTIAL WORK MARKS VISIBLE AT APPROXIMATELY 20X MAGNIFICATION UNDER A LIGHT MICROSCOPE.
6. ALL DIMENSIONS IN INCHES.
7. TOLERANCES: .xxx=0.005, .xx=0.030 UNLESS OTHERWISE SPECIFIED.
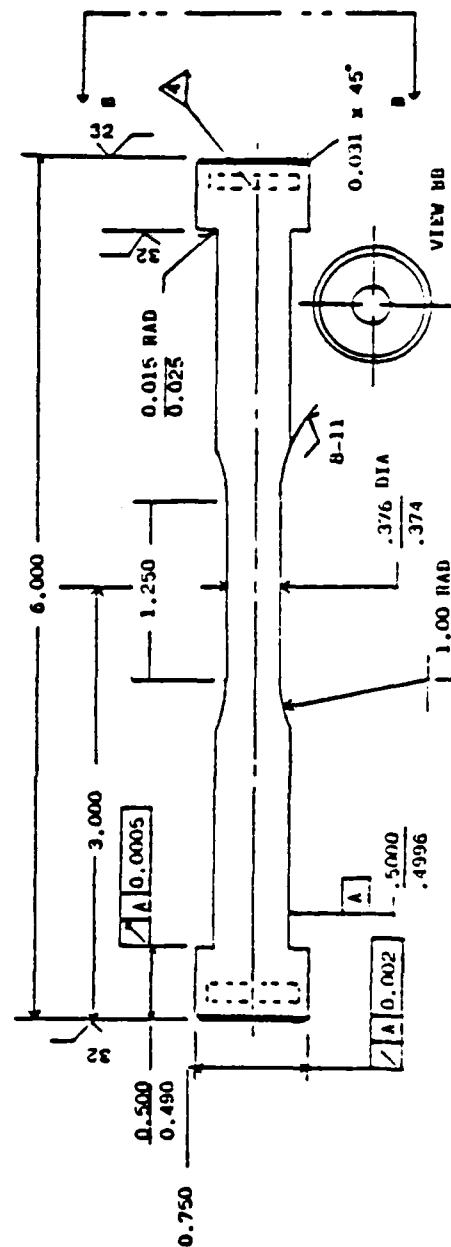
Figure 3.5   Specimen Geometry and Machining Procedure.

insulation was coated with Liquid Paper. This minimized the formation of loose fibers of insulation, which can obscure the specimen surface when examined on the SEM.

2. **MTS Preparation**

The MTS testing equipment was prepared for the sample as follows;

a. Electronic Controls

The range scales were set as indicated in Table IV.

	TABLE IV	
	Range Scales	
Parameter	Percent Range	Correspondence
Load	50	1000 lb/volt
Elongation	10	.002 in/volt
Stroke	50	.25 in/volt

The function generator was then set to produce a strain rate of 4×10^{-3} sec^{-1} by means of reversing ramp function with a rate of 2 volts/sec, Figure 3.6. The peak values were determined by setting the break point percent adjustment. For example, to obtain total strain range of 0.005, the break point adjustment was set at 1.25, which yields a peak voltage of ±1.25 volts, which inturn corresponds to an elongation of ± .0025 inches, or a total Strain of .005. To conduct a subsequent test, the only adjustment required was to the break point.
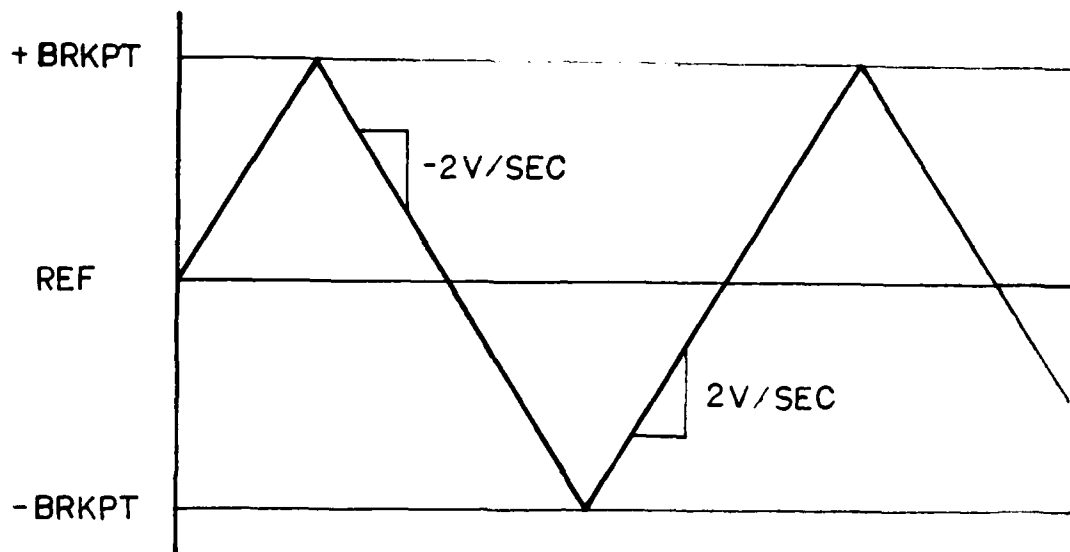
35

Figure 3.6   MTS Function Generator Output Voltage.

    b.   Protection Devices

        The approximate values used for trip set points for the protection devices are summarized in Table V.

TABLE V

Protection device trip points

Protection Device	Set Point
Over Load	120% of peak load during cycling
Strain	120% of peak strain
Stroke	0.5 inches from null
Temperature	50 degree C deviation
Under Peak	75% of peak load during cycling

36

To set the overload and underpeak interlocks, the specimen was cycled with the overload interlocks set well above the expected load and the underpeak interlocks deenergized. When the hysteresis had stabilized subsequent to strain hardening, the peak load values were recorded and the underpeak and overload interlocks were adjusted. The underpeak detectors were only activated during actual cycling, since they will normally trip when the cycling is started or stopped. The underpeak detectors act to shut down the test when the reduction in area due to the crack was approximatly 50%, which was considered the end of fatigue life, for these tests.

3. Specimen Testing Procedure

The specimen was inserted in the coil and attached to the MTS grips. The specimen was hydraulically locked into the grips as described in Reference 26. The extensometer was installed with slightly less than one inch (2.54 cm) distance between contact points to allow for thermal expansion. This was accomplished by using the strain error signal from the MTS controller, and at cycling temperature the error was consistently less than .003 inches and normally less than .001 inch. Two small areas of the gage length were covered with Liquid Paper and these were the contact points of the extensometer rods. This was necessary due to slippage problems of the extensometer rods on the smooth surface of the gage section. The specimen was heated at a rate of about 4 °C/sec and the coil was adjusted to give a controlling signal and reference signal as per the coil calibration data. The controlling thermal couple was on the upper gage fillet and the reference thermal couple was on the lower one.

After a fifteen minute wait to stabilize temperature, the load was zeroed using the set point adjustment,

37

and the strain signal was electrically zeroed on the associated controller module. The overload (initially set well above expected peak loads), over strain, and over stroke interlocks were energized, and the MTS controller was switched to strain control. Of note is that, for these experiments, the total strain range was imposed from the first cycle and therefore, considerable plastic strain was induced. As the specimen strain hardened, the hysteresis loop narrowed and gained in height, indicating less plastic strain as a result of strain hardening. Figure 3.7 shows typical hysteresis loops during the first few cycles. When the hysteresis loop stabilized, the overload and underpeak interlocks were adjusted and the underpeak interlocks were energized.

4. Hysteresis Matching

Since most of the tests were conducted under conditions resulting in significant plastic strain, it was necessary to develop a procedure to match hysteresis behavior before and after the test interruption and examination, as if cycling were continuous. To accomplish this, the test was always stopped as the strain reached zero from negative values. The load therefore was positive and increasing. The hysteresis of the cycle just prior to interruption was recorded on the X-Y recorder and the load voltage was recorded just after the test was interrupted. The MTS controller was switched to load control and the load was reduced to zero. The specimen was cooled at a rate of approximately 1 °C/sec, and removed for examination. Upon reinitiation of the test, the procedure above was followed. After the 15 minute hold period, the load was increased to the load recorded just after test interruption and the strain was zeroed. The controller was switched to strain
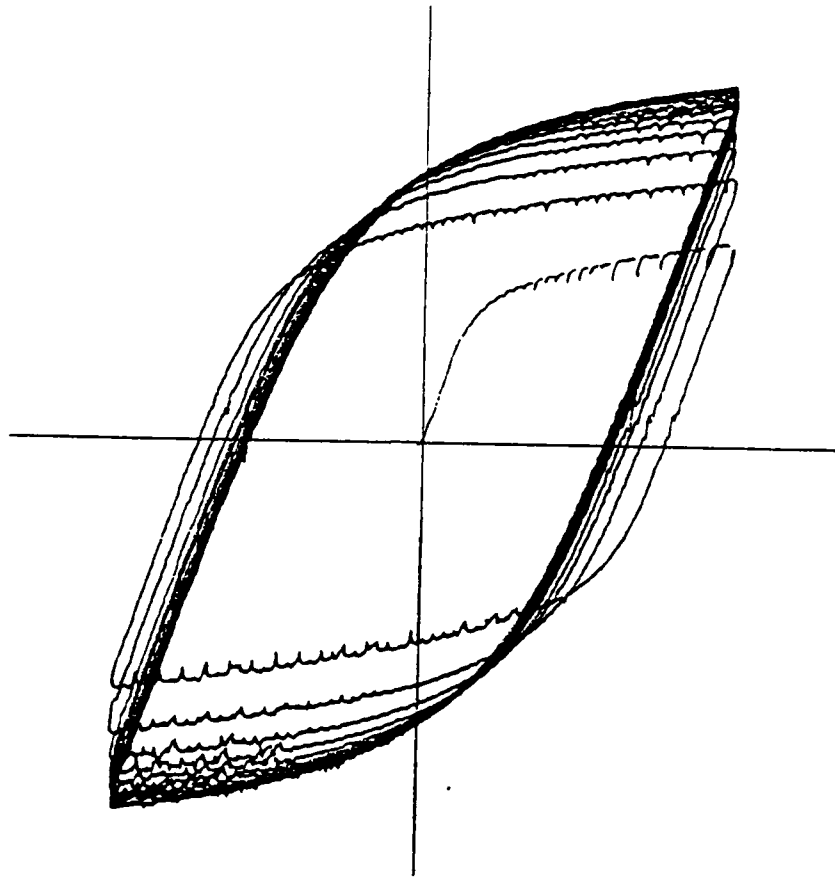
38

Figure 3.7   Typical Hysteresis Loops with Strain Hardening.

control,   the   X-Y recorder was   started and   cycling began.
This superimposed the hysteresis of cycles after the inter-
ruption cn to that just prior to the interruption.   This
gave immediate indication of how well the two matched.   With
the   exception cf scme softening,   the   hysteresis   loops
matched and within a few cycles, strain hardening brcught
the new hysteresis lcop to coincide with those pricr to test
interuption.

        Without this procedure, the plastic strains left in
the   sample when   the test   was interupted   would have   been
cumulative, and would have made the results suspect.

5. Scanning Electron Microscope Procedure

The specimen was placed in the SEM stage with the top end (as loaded in the MTS) oriented away from the feed-through flange. The specimen was moved to center the upper thermal couple on the SEM screen, and the indices of the axial and rotational feed-throughs were recorded. This gave a repeatable reference point for viewing the specimen gage length. At 20X nominal magnification, the entire gage length was mapped in a 50 frame matrix (10 frames axial by 5 frames radial). The matrix was labeled using the indices from the feed-throughs, so that a single spot on the sample could be repeatedly examined as more and more cycles were accumulated by the specimen.

The viewing procedure used was to examine the entire gage length at 20X nominal. Any area that looked promising for a crack was examined at higher magnification. If a crack or possible initiation site was found, a micrograph was taken and the area was marked on the map, for subsequent comparison as cycles increased and crack growth progressed.

D. SPECIMEN SECTIONING FOR OPTICAL MICROSCOPY

One specimen was sectioned into two semicylindrical halves, each containing a portion of the major fatigue crack, as shown in Figure 3.8. This allowed a profile view of the crack with one section and examination of the oxide layer and associated substrate on the other. One of the halves was mounted, curved surface down. A flat was ground on the curved surface using a Buehler Surfmet II with an 80 grit belt, then a 180 grit belt, and successively ground by hand on 240, 320, 400, and 600 grit paper. The specimen was polished in three steps on Buehler polishing wheels and then etched with 2% Nital solution. The surface was repolished on the final wheel and re-etched in the same solution. This

40
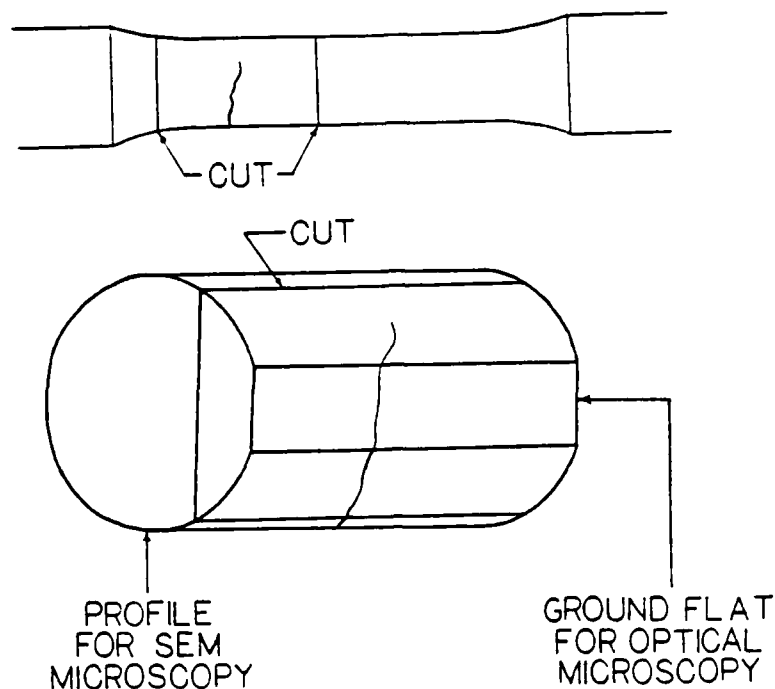
Figure 3.8   Specimen Sectioning Diagram.

procedure geometrically magnifies the oxide layer since a
short cord was ground on the cylindrical surface.   This
allowed detailed microscopy of the oxide layer at lower
magnifications, which is recessary due to the rounding of
the edges of the specimen as a consequence of the polishing
procedure.   The specimen was then examined optically on a
Zeiss Cptical Microscope.

The longitudinally cut surface of the other half was
ground and polished in a similar manner except that the two
belt grinder steps were omitted.   The specimen crack was
coated with lacquer to prevent damage in the subsequent
polishing and etching.   The specimen was polished, etched,
polished and re-etched as above.   The lacquer was dissolved

41

in acetone and the profile of the fracture path was examined
on the Cambridge SEM.

IV. RESULTS

A. GENERAL

Determination of the cycles to crack initiation has uncertainty, since the method used would only bracket the actual number of cycles to crack initiation. Additionally, there is uncertainty that the first crack observed was in fact the first crack initiated. In general, a crack would be first observed early in the propagation stage, and the initiation point was assumed to occur at the number of cycles of the previous examination. In one specimen (specimen #25 tested at a 0.4% total strain), the crack had propagated substantially (about a 60° arc length) before it was detected. The initiation point in this specimen was extrapolated using crack growth information from specimen #31 (1% total strain) and specimen #18 (0.5% total strain). In another specimen (specimen #24 tested at 0.35% total strain), failure occurred at the specimen grip during the propagation stage. The number of cycles to failure was extrapolated by again using crack growth information from specimen #31 (1% total strain). These extrapolations assumed that the fraction of the number of cycles for propagation of a crack to a given arc length, divided by the total cycles of propagation, was the same for all specimens. Details of the extrapolations are given in Appendix A for each specimen.

B. SPECIMEN TEST RESULTS

Six specimens were successfully tested to completion. Five specimens were unsuccessful for reasons as follows: Two buckled, one necked due to a procedural error, and one

43

necked presumably due to slippage of the extensometer and
then buckled, and one fatigue cracked at a thermocouple
spotweld. Additionally, three button heads failed due to
fatigue cracks initiated at the fillet. However, a thread
was machined on the specimen shank and a thread type grip
was used to continue testing. One of these screw ends
failed due to fatigue initiated by the threads before
failure was obtained on the gage length. One of the unsuc-
cessful specimens, (specimen #14) provided a lower limit to
crack initiation at 0.3% total strain and is therefore
included in the results. Appendix A contains detailed
descriptions of the specimens included in this thesis and
micrographs obtained during testing. A summary of the
results obtained are contained in Table VI.

TABLE VI
Summary of Results

Specimen Number	Total Strain(%)	Number of Cycles to Initiation Nn	Number of Cycles to Failure Nf	Nn/Nf
Tests without Dwell				
31	1.00	574	1049	0.453
15	0.80	650	1430	0.455
18	0.50	3300	5322	0.620
25	0.40	9900[1]	12376	0.800
24	0.35	29236	39300[1]	0.744
14	0.30	>79908		
5 Miniute Maximum Strain Dwell				
32	0.50	<300	1949	<0.154

[1] Extrapolated from crack growth data from Specimen #31

These results are plotted as total strain vs. number of cycles, superimposed on data from hour glass shaped specimens generated by ORNI, shown on Figure 4.1. Notice that Nf for the uniform gage length specimens of this thesis is always less than Nn for the hour-glass shaped specimens. Hour-glass shaped specimens will have the oxide crack with subsequent initiation at the point at minimum diameter. Since oxide cracking is caused by random defects in the oxide layer, the number of cycles to oxide cracking and crack initiation in the substrate is expected to be larger than for a uniform gage length type specimen, as the likelyhood of a crack initiating defect in the oxide is increased due to the greater volumn of uniformally stressed oxide in a sample with uniform geometry.

Figure 4.2 shows Nn/Nf plotted against total strain, superimposed on the estimate proposed by Challenger [Ref. 7]. The experimental data for Nn/Nf was generally to the right of that predicted by Challenger, but the general trend was the same, and a best fit line is nearly parallel to the predicted curve. Due to the few number of data points, the statisical nature of oxide cracking and subsequent crack initiation, and uncertainties associated with Nn, a better plot of Nn/Nf verses total strain connct be constructed. Therefore, the estimate of Challenger [Ref. 7] should be used until further research can refine the relationship.

C. CRACK MICROSCOPY

Appendix A.2 contains micrographs of cracks that have propagated into the substrate. There are numerous examples as well, of oxide cracks leading to the formation of oxide "fingers" also penetrating the substrate, but no evidence whatsoever that cracking occurred in the substrate first.

45
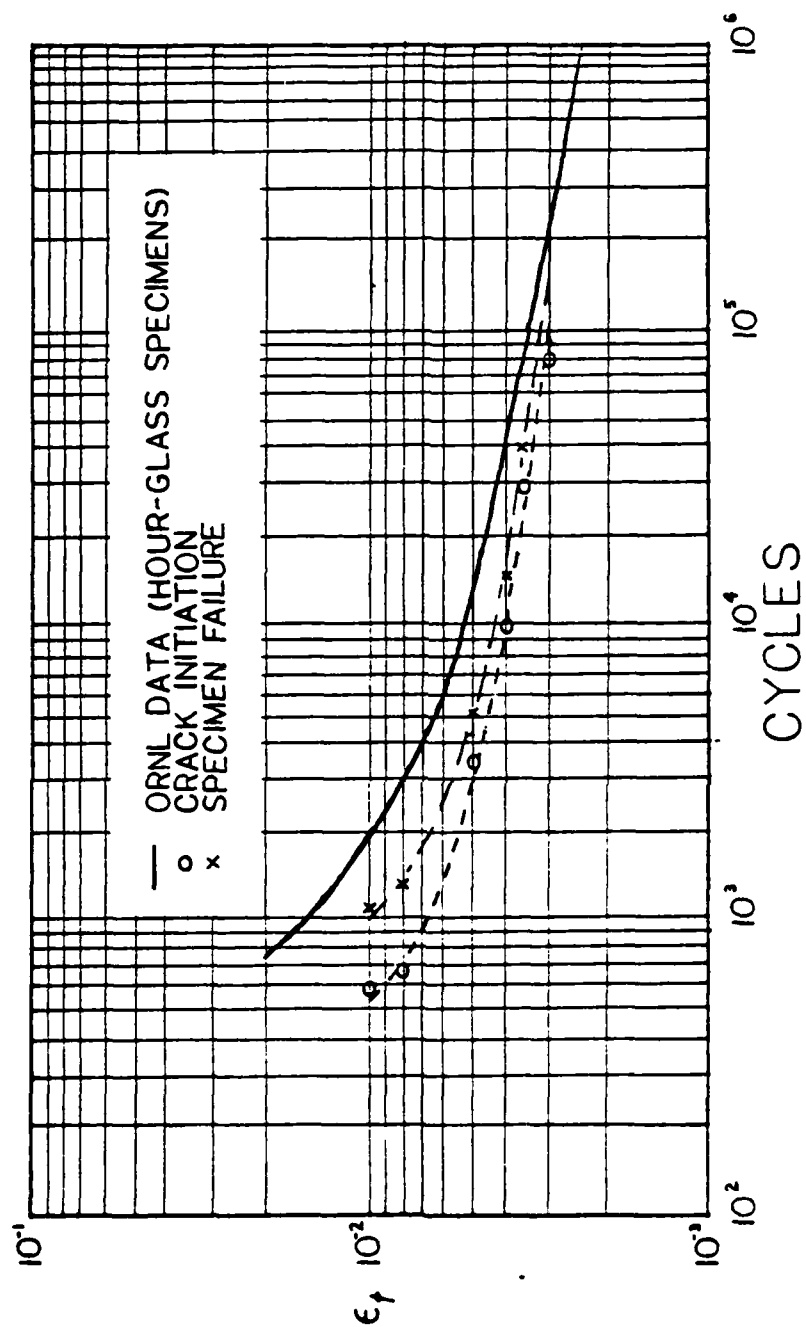
Figure 4.1   Nn and Nf verses Total Strain Range.

46
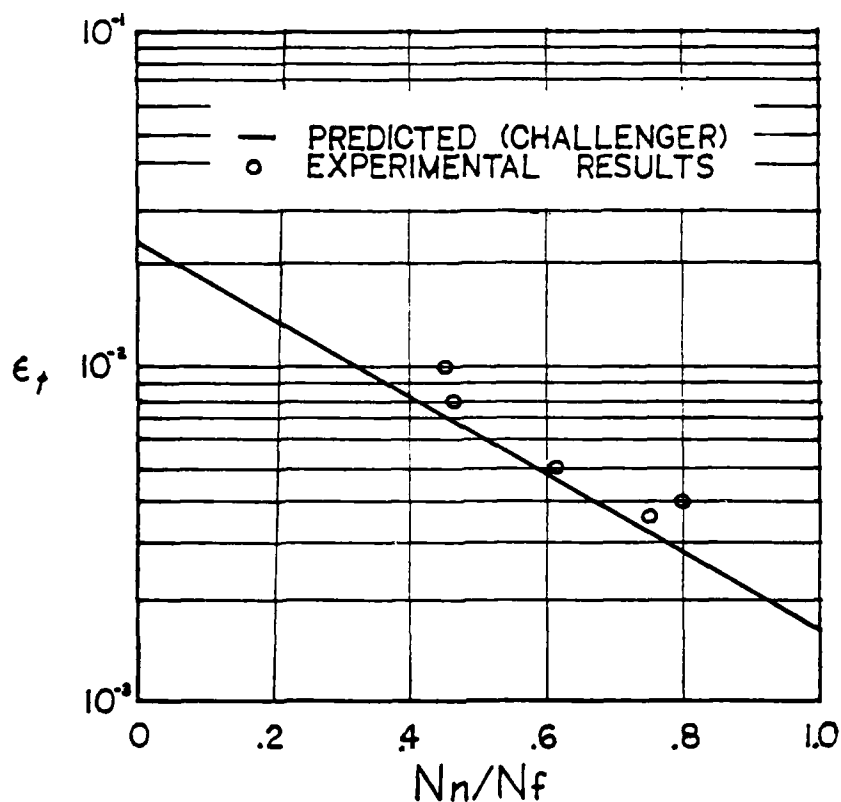
Figure 4.2 Nn/Nf verses Total Strain.

In particular, there were no steps at the interface to indi-
cate that the crack could have been initiated by a persis-
tent slip-band i⁻ ⁺he substrate, and no evidence of cracking
in the substrat   ᵗhout associated cracking of the cxide
layer. Further, cracks appear to occur randomly both in
grains and at grain bcundaries.   This again indicates that
the crigin of the cracks was the oxide and not the
substrate.

    The cracks which were formed are in general transgran-
ular, cutting through both pearlite and ferrite grains.
This was confirmed by both optical and SEM examinaticns, and

47

is consistent with the findings of Armitt et al [Ref. 13] as well.

D. SPECIMEN WITH COMPRESSIVE DWELL

With a compressive dwell, two factors tend to promote oxide cracking and subsequent crack initiation earlier in fatigue life. First, the time at temperature and therefore oxide growth per cycle is greater. For comparison, the time at temperature to failure of specimen #18 (0.5% total strain without dwell), equates to approximately 63 cycles on specimen #32 (0.5% total strain with a five minute compressive dwell). Second, the oxide grows at a "stress free" state while the substrate is in compression. When the cycle is completed after the dwell, the oxide is subjected to a longitudinal tensile strain equal to the total strain range. This produces circumferential cracks in the oxide, which surve to initiate the crack in the substrate. Detailed description of specimen #32, tested with a five minute dwell at maximum compression and a total strain range of 0.5%, is contained in Appendix A, with a summary included in this section. At 300 cycles, numerous circumferential cracks were observed throughout the gage length, with crack penetration visible into the substrate. Substrate cracking had clearly deeped at 595 cycles. Clearly the oxide cracking promoted crack initiation into the substrate since the number of cycles to crack initiation was at least a factor of 11 lower than that for specimen #18, which was cycled without dwell at the same strain range. Additionally, examination of the fracture surface for the continuously cycled specimens indicated a single crack initiation origin, with the crack front concaved toward the origin. In this specimen with the compressive dwell, initiation occurred on numerous sites. These cracks joined to produce a single

48

crack front convex toward the initiation sites. This is
typical of a fatigue crack front found on a shaft with a
circumferential groove. This clearly indicates that the
crack initiation is directly caused by the oxide cracks
which profusely form with compressive dwell periods. Since
fatigue loading history of this material in service is vari-
able and unknown, it is reasonable to expect that crack
initiation can occur very early in the life of the compo-
nent. Therefore, fatigue life estimations which lump
together the crack initiation and propagation stages are
likely to be erroneously high.

V. CONCLUSIONS AND RECOMMENDATIONS

A. CONCLUSIONS

The results of this thesis leads to the following conclusions:

1. Oxide cracking promotes crack initiation

In all specimens tested, oxide cracking was a precursor to the initiation of a crack in the substrate. In particular, sample #32 tested with a 5 minute maximum compressive dwell period had an initiation point decreased by a factor of at least 11 compared to sample #18 which had no dwell period. Additionally, the fracture surface showed that the crack initiated on numerous sites on the circumference of the specimen. These individual cracks grew together and produced a single crack, with the crack front convex toward the specimen surface. All specimens tested without dwell had a single crack initiation site and the front of the crack was concaved toward the origin. These affects are directly attributable to the enhanced cracking in the oxide layer resulting from the dwell, proving that fatigue crack initiation is caused by oxide cracking.

The mechanism for fatigue crack initiation is thought to proceed as follows: The oxide cracks, exposing the substrate material to the air, causing localized and accelerated corrosion. On the next cycle, the oxide is again cracked and oxide "fingers" grow into the substrate. The effect of this mechanism is to initiate the crack and increase the crack propagation rate, in agreement with the results of this thesis.

2. Crack Propagation is Transgranular

In examination of the profile of the cracks, all cracks were found to be transgranular, cutting across both pearlite and ferrite grains. This is consistent with the findings of Armitt [Ref. 13].

3. Fatigue Life Calculations Must be Based on Propagation

In service, oxide growth and cracking is a function of time, temperature, and fatigue loading history. Since the fatigue loading history is variable, oxide cracking and subsequent crack initiation can be expected very early in the component's life (ie first few thermal cycles). Clearly, estimations of fatigue life based on lumped crack initiation and propagation stages experimentally generated in the laboratory, can be a drastic overestimation. Therefore, estimations must be based on the crack propagation characteristics of this material to be valid under operational conditions.

B. RECOMMENDATIONS

Much can be done as a follow on to this work. The following recommendations are made:

1. Modify the Specimen Geometry

Most of the specimens which were unsuccessfully tested had problems arising from the specimen geometry. The buckling problem was found to be due to an oversized button head diameter, which caused a slight cocking of the specimen when inserted. This can be eliminated by making the button head diameter 0.745 ±.002 inches. Secondly, the button head fillet radius must be increased to 0.040 ±.005 inches, to prevent fatigue cracking in the fillet region.

51

2. Conduct Further Tests at 538 °C

Since fatigue is statisical in nature, further tests and 538 °C need to be performed to refine the data of this work, particularly for total strain ranges less than 0.05%.

3. Conduct Tests at Other Temperatures.

To further study crack initiation of this alloy, further tests need to be conducted at other temperatures. A temperature of 427 °C is recommended since extensive fatigue fracture data is available from the ORNL tests. In addition, Challenger [Ref. 7] has extrapolated the N_n/N_f versus total strain range for this temperature. This gives data for comparison of the results obtained.

4. Study Short Crack Growth

Most of the crack growth data for this material has been on long cracks where LEFM is valid. Detailed analysis of short crack growth needs to be performed to be able to accurately predict fatigue life based on the crack propagation stage alone, as recommended above.

5. Study the Effects of Coatings

Further research on the effects of coating and surface treatments such as shot peening needs to be performed. This would give information concerning their effects on the crack initiation phase in fatigue, possibly resulting in an extended fatigue life of components made of this alloy.

APPENDIX A
SPECIMEN DATA

1. SPECIMEN #31- 1% TOTAL STRAIN

Specimen #31 was cycled with a total strain range of 1%. The test was interrupted and examined at 250, 325, 400, 475, 550, 625, 775, and 925 cycles. At 475 cycles one area showed oxide layer cracking as shown in Figure A.1. Examination of the area at higher magnification showed oxide cracking but no confirmed cracks in the substrate, Figure A.2. At 550 cycles a crack was clearly visible at 95X, Figure A.3, confirming that the crack did initiate at about 475 cycles and was now propogating. At 775 cycles, the crack had grown substantially, Figure A.4. By 925 cycles, the crack was visible to the unaided eye, Figure A.5. Note also that substantial secondary cracking was occuring near the major crack, Figure A.6. There was one other area monitored that showed a fatigue crack in earlier stages of formation. Figure A.7 shows this area at 625 cycles, Figure A.8 shows that the crack is propagating at 775 cycles and Figure A.9 shows the same crack at 925 cycles. Note that all micrographs of this area show the same banana shaped spot to the right of the crack, which served as a benchmark.

Figure A.10 shows an interesting defect in the oxide layer. There were several of these lines oriented at about a 30° angle to the specimen axis, and distributed throughout the gage length. None of these showed oxide cracking throughout the specimen's life and their origin is unknown. Failure of the specimen occurred at 1049 cycles.

53
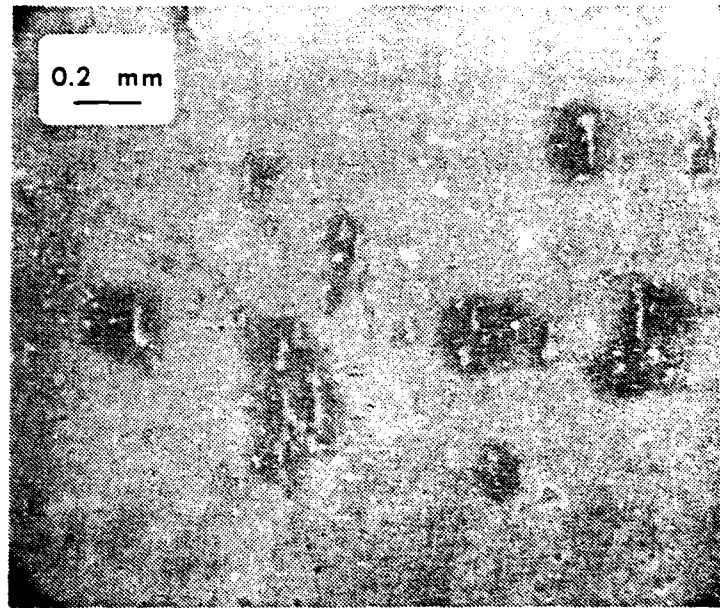
Figure A.1   Specimen #31   475 Cycles.
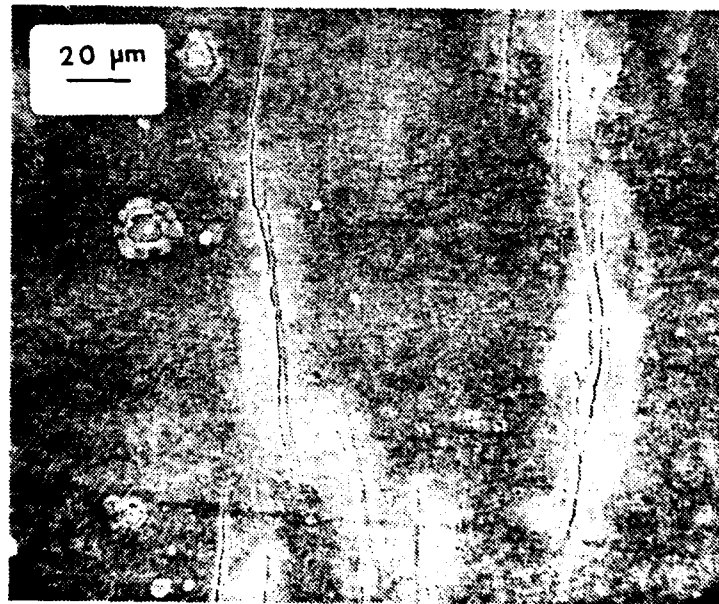
Figure A.2   Specimen #31   475 Cycles.

54

0.1 mm
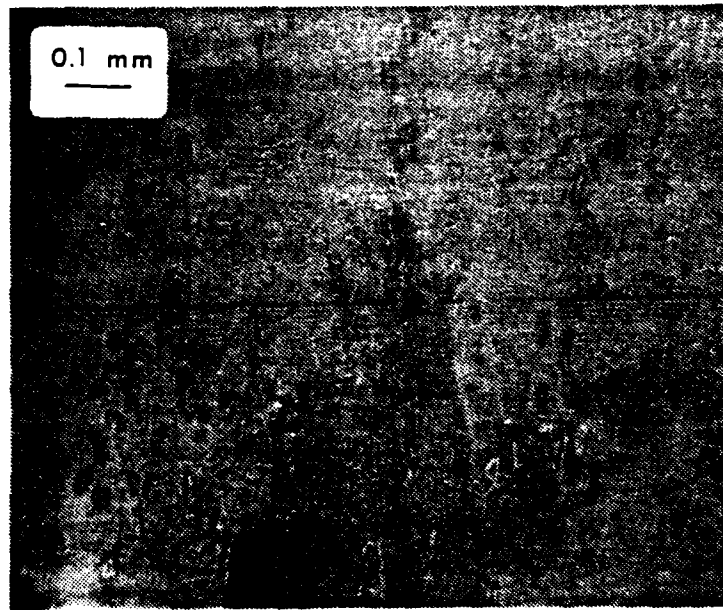
Figure A.3   Specimen #31   550 Cycles.

50 µm
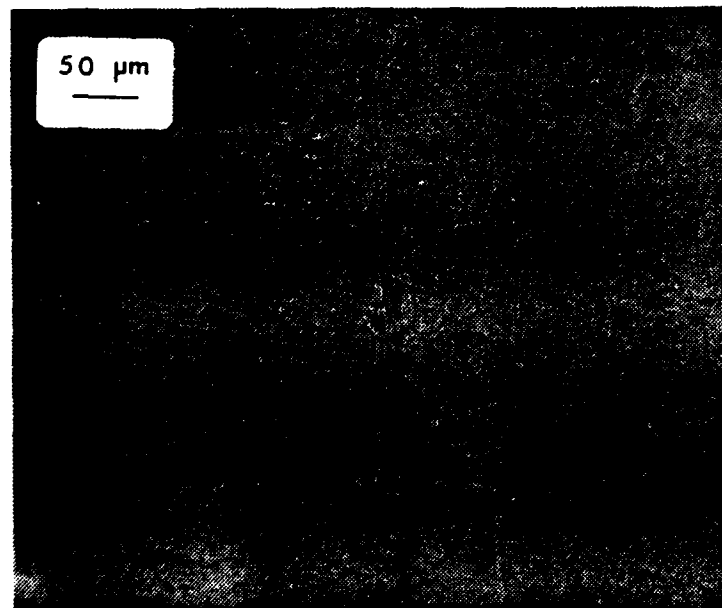
Figure A.4   Specimen #31   775 Cycles.
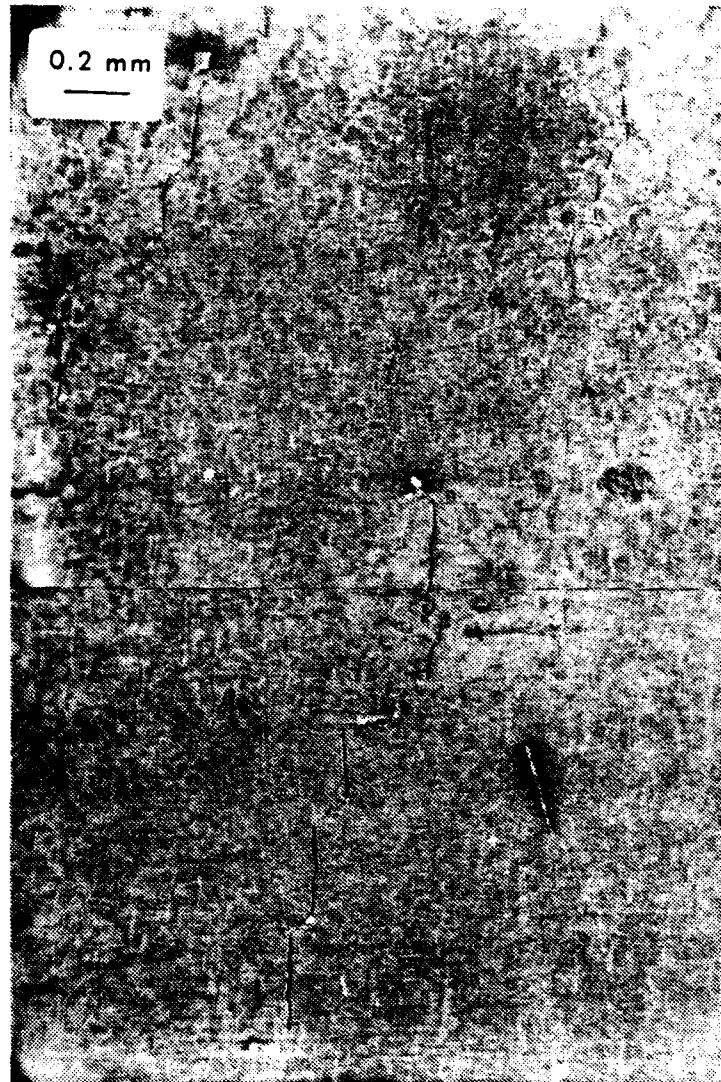
Figure A.5   Specimen #31   925 Cycles.

0.5 mm
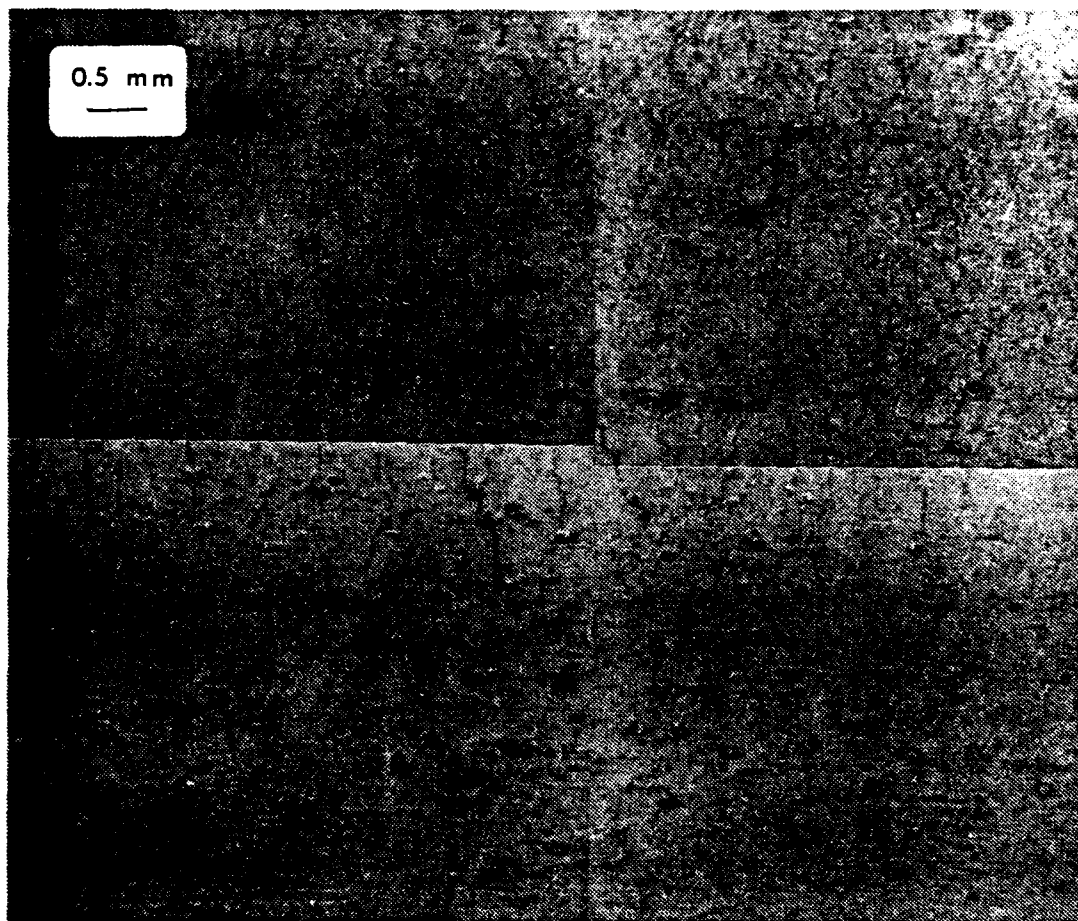
Figure A.6   Specimen #31   925 Cycles.

20 μm
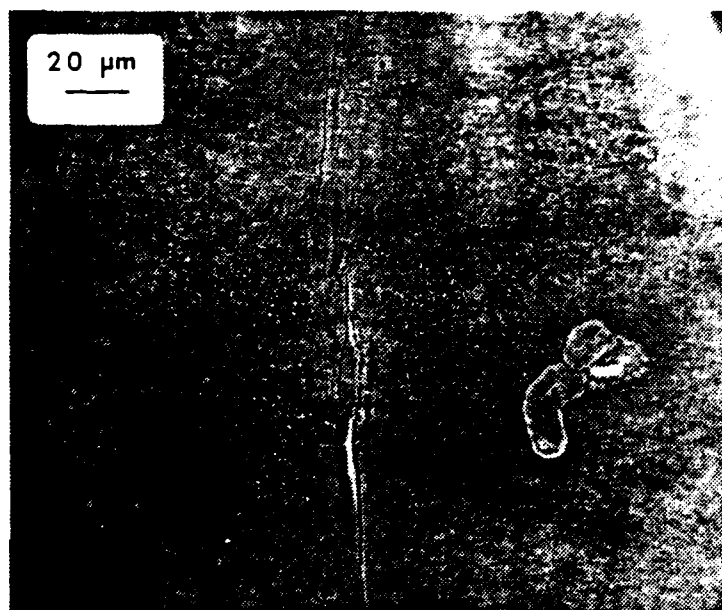
Figure A.7   Specimen #31   625 Cycles.
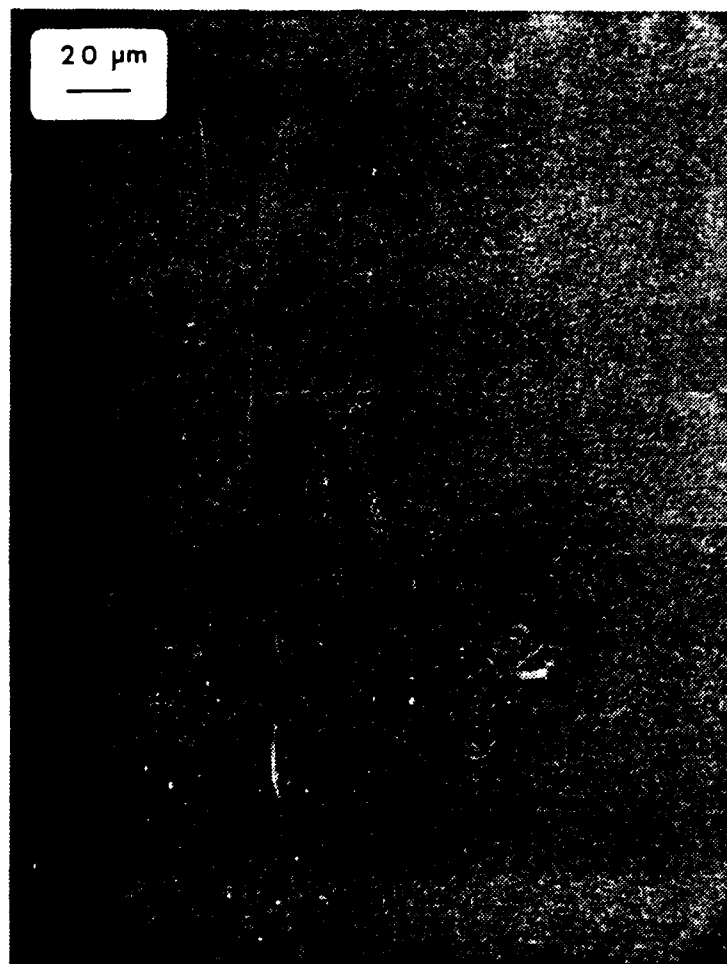
Figure A.8   Specimen #31   775 Cycles.
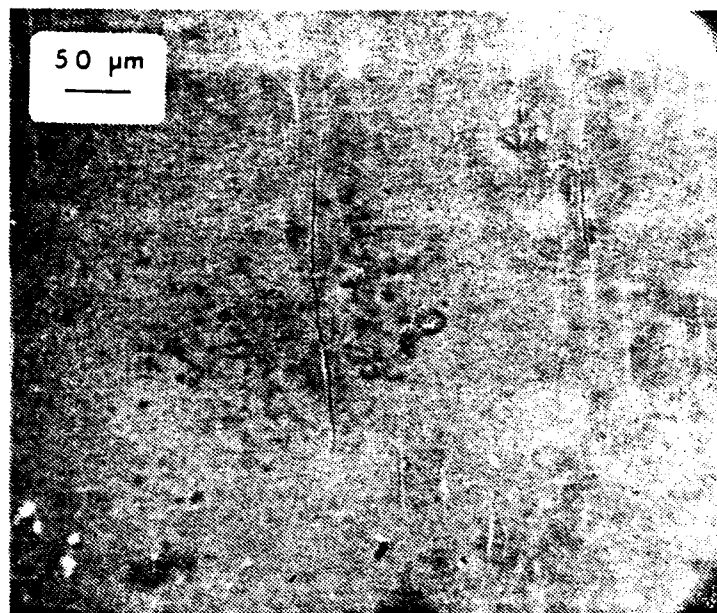
Figure A.9   Specimen #31   925 Cycles.
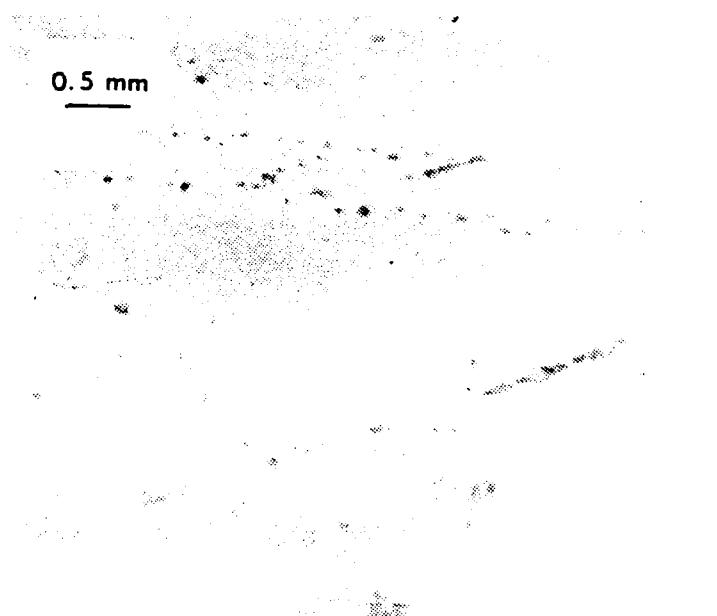
Figure A.10   Specimen #31   Oxide Defect.

60

2. SPECIMEN #15 0.8% TOTAL STRAIN RANGE

Specimen #15 was continuously cycled with a total strain range of 0.8%. The test was interrupted and the specimen examined at 500, 550, 600, 650, 700, 750, and 850 cycles. The specimen appeared smooth and featureless until 600 cycles, at which time some oxide cracking had occurred in one area. Figure A.11 shows a representative crack at a magnification of 1800X. Figure A.12 shows the same crack at 650 cycles, with no change, and the area in general showed more severe oxide cracking, but no crack growth. The crack initiation occurred at about 650 cycles, since the crack had clearly penetrated the substrate, and was propagating at 700 cycles, as shown in Figures A.13 to A.15. At 750 cycles the crack had further propogated, Figures A.16-A.19. At 850 cycles the crack had grown and widened further, Figures A.20-A.22. The specimen was then continuously cycled to failure, which occurred at 1430 cycles.

A composite micrograph of the failed area was made in preparation for sectioning the specimen. Figure A.23 shows the result. Note that the crack extended around the specimen, making an arc of approximately 200°. The specimen was sectioned and a cord was ground on a portion of the cylindrical gage length and prepared for optical microscopy as discussed in Section III.D. This gave a geometrical oxide magnification factor of approximately three. Figures A.24 to A.35 show the details of the oxide and associated substrate. Notice the oxide "fingers" growing into the substrate where the oxide has been breached by a crack. There is no evidence of cracking within the substrate without associated cracking of the oxide layer, or steps on the interface which could have been caused by persistent slip bands within the substrate. The oxide "fingers" appear to be randomly distributed along the surface, showing no

61

preference to grain boundary or intergranular formation. This indicates that cracking of the oxide layer is a precursor to crack initiation..

Examination of the cracks, Figures A.35 and 6aabc show that the cracks propagated transgranularly, cutting both pearlite and ferrite grains. Scanning Electron Microscope examination of the profile of the crack revealed similar findings, Figures A.36 to A.41. Figure A.36 shows one such crack that is less than one grain diameter in length.
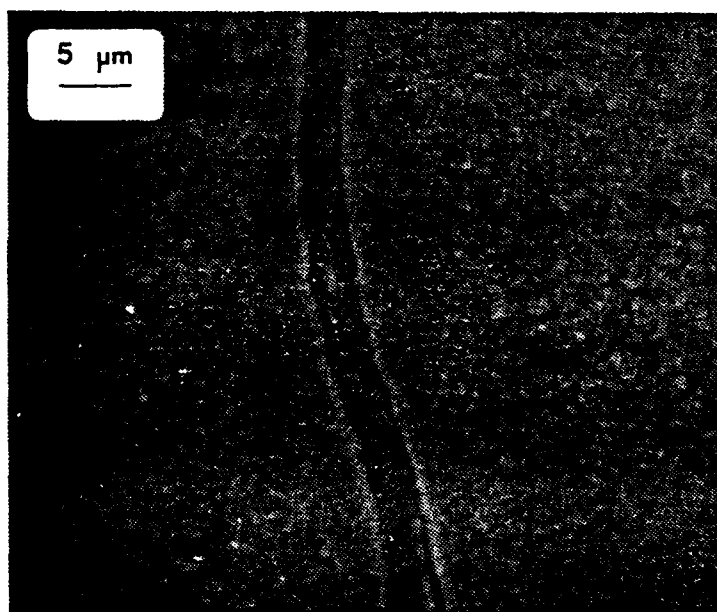
Figure A.11   Specimen #15   600 Cycles.
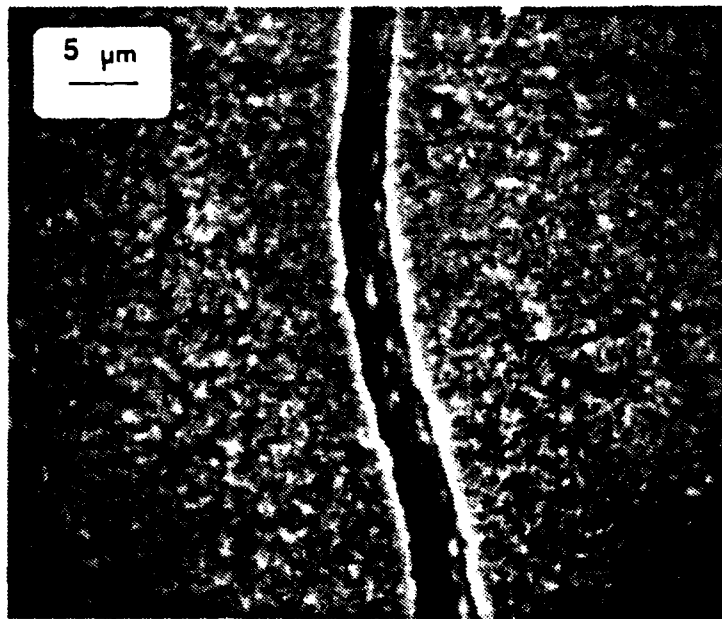
Figure A.12   Specimen #15   650 Cycles.
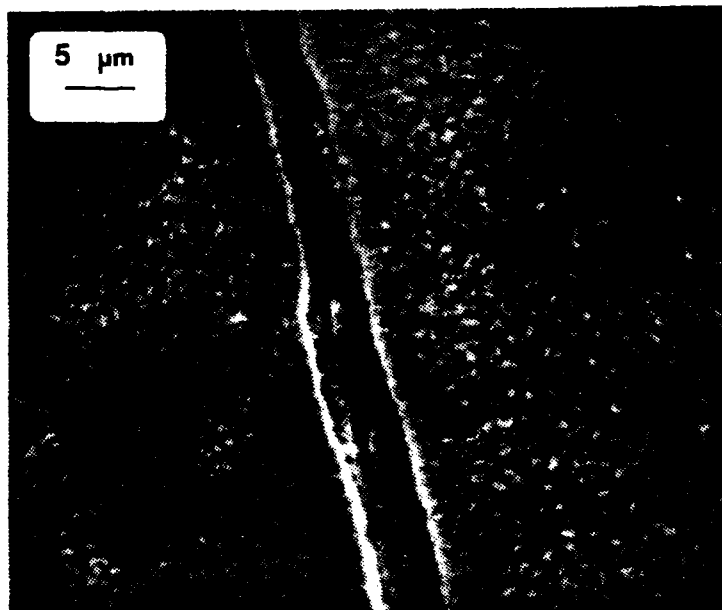
Figure A.13   Specimen #15   700 Cycles.

63
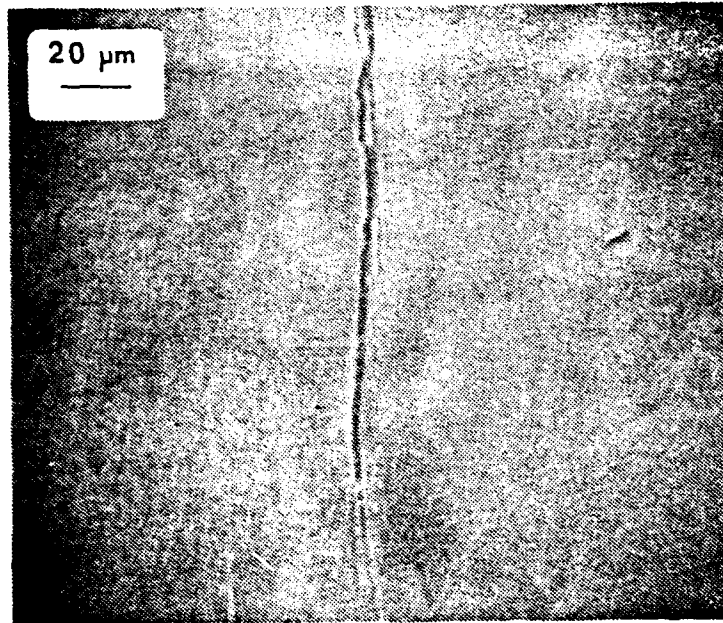
Figure A.14   Specimen #15   700 Cycles.
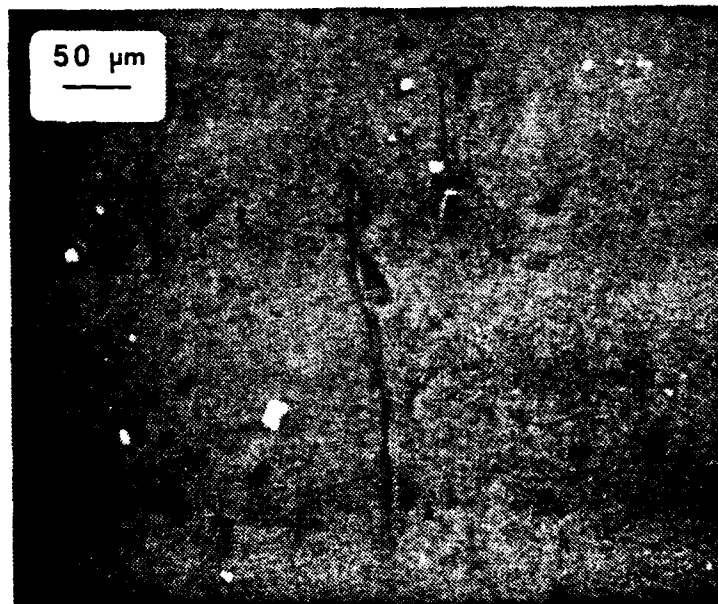
Figure A.15   Specimen #15   700 Cycles.
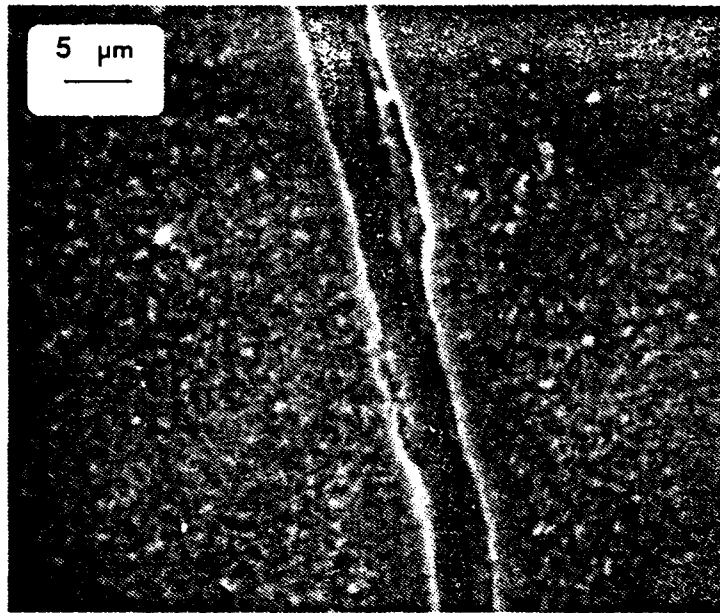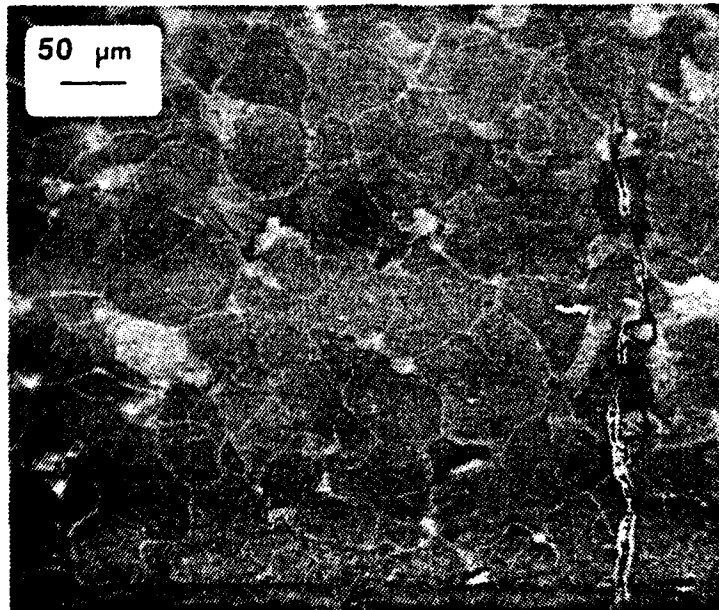
Figure A.16   Specimen #15   750 Cycles.
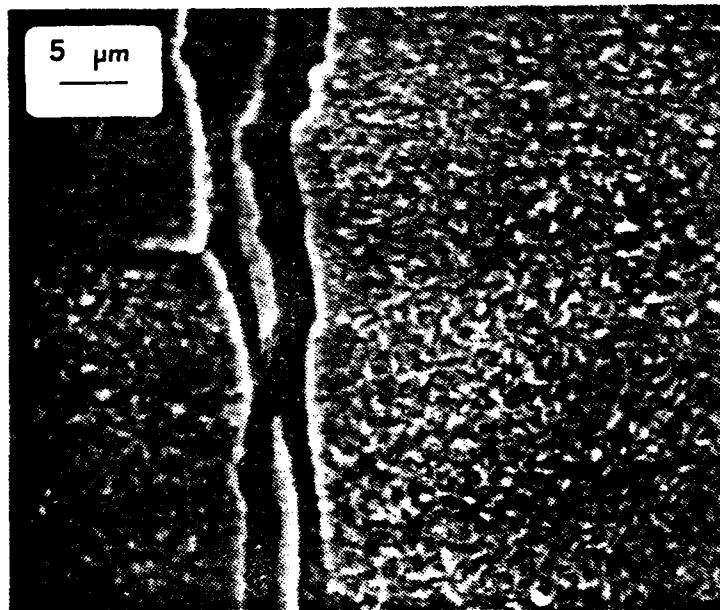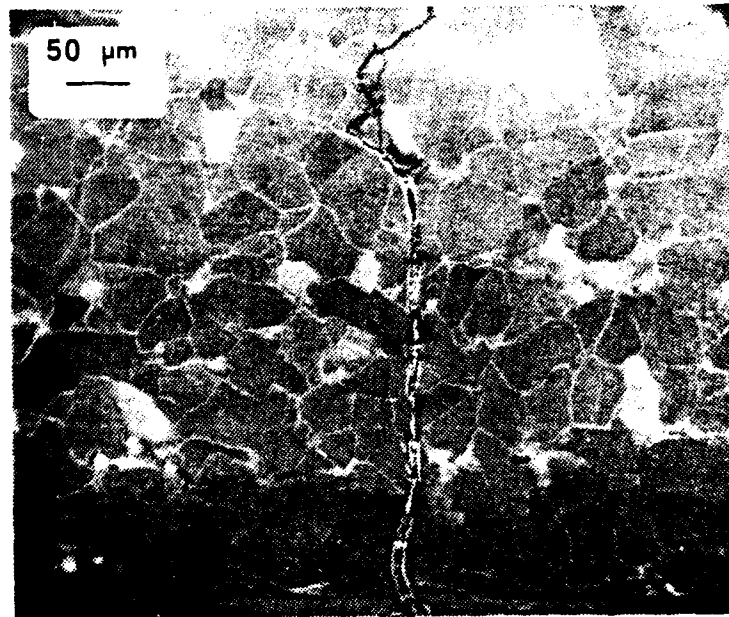

Figure A.17   Specimen #15   750 Cycles.

65
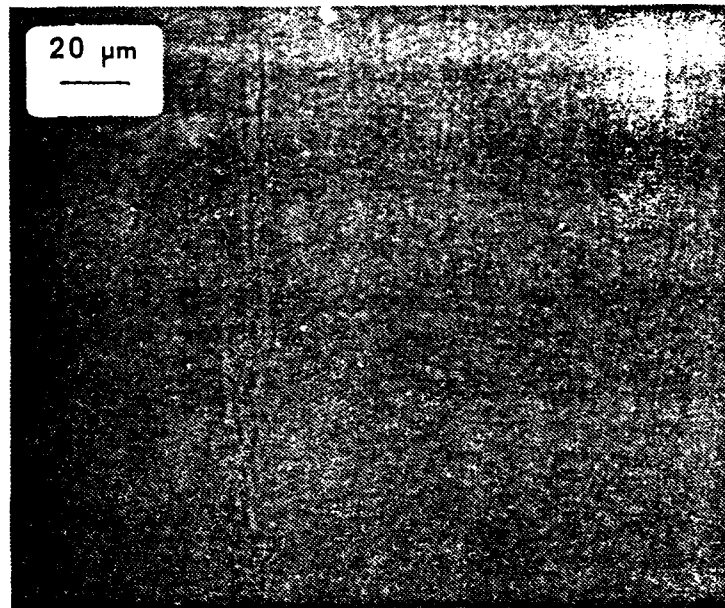
Figure A.18   Specimen #15   750 Cycles.
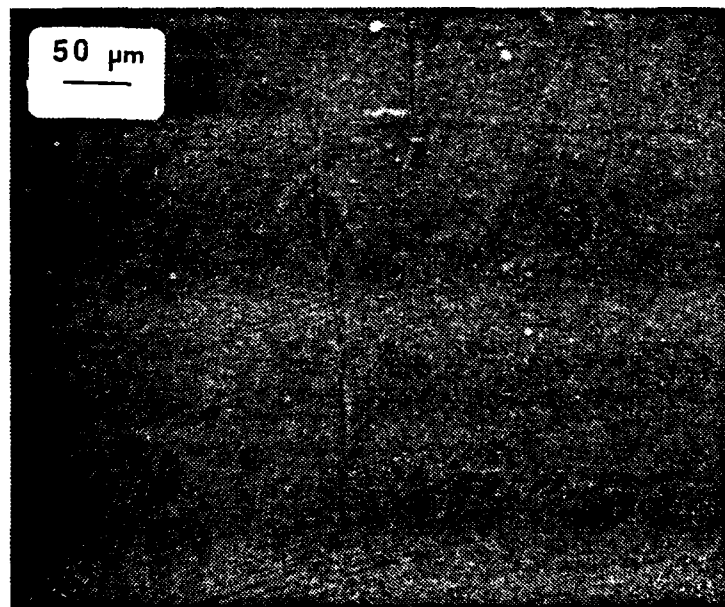
Figure A.19   Specimen #15   750 Cycles.
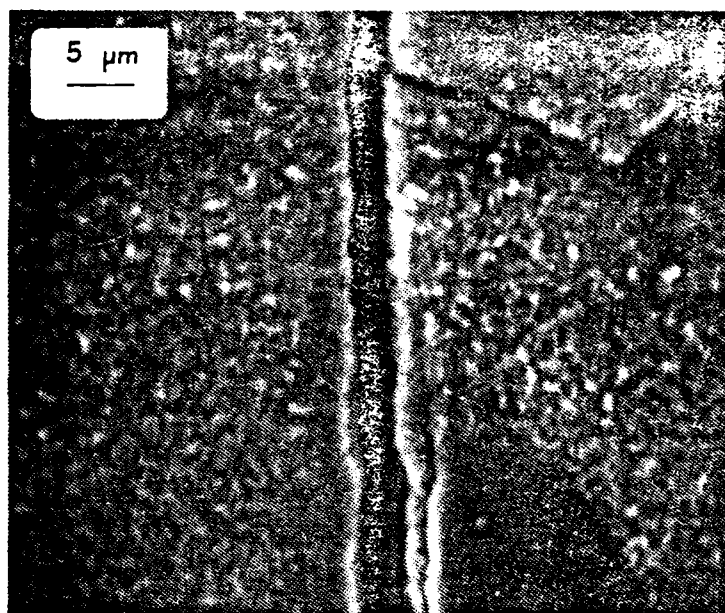
Figure A.20   Specimen #15   850 Cycles.
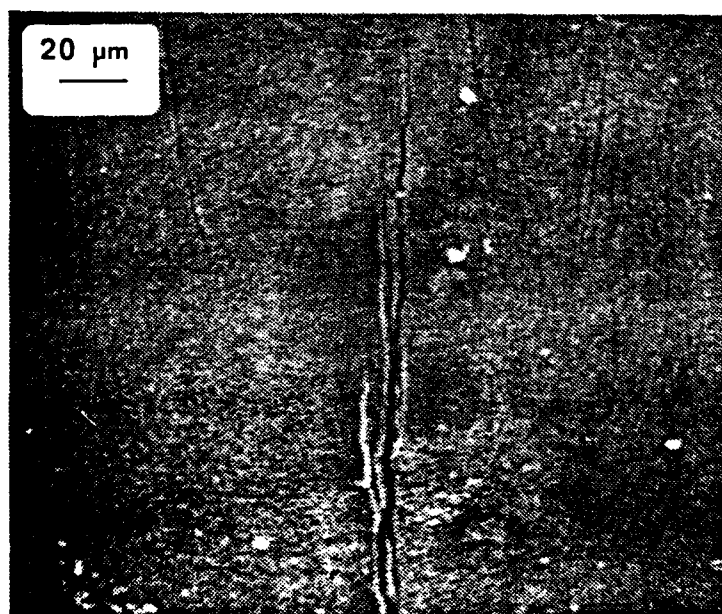
Figure A.21   Specimen #15   850 Cycles.

50 µm
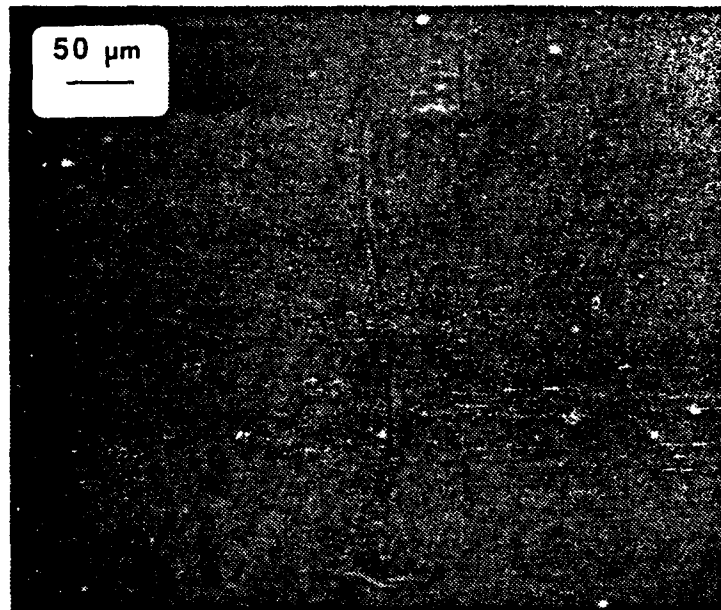
Figure A.22   Specimen #15   850 Cycles.

0.2 mm
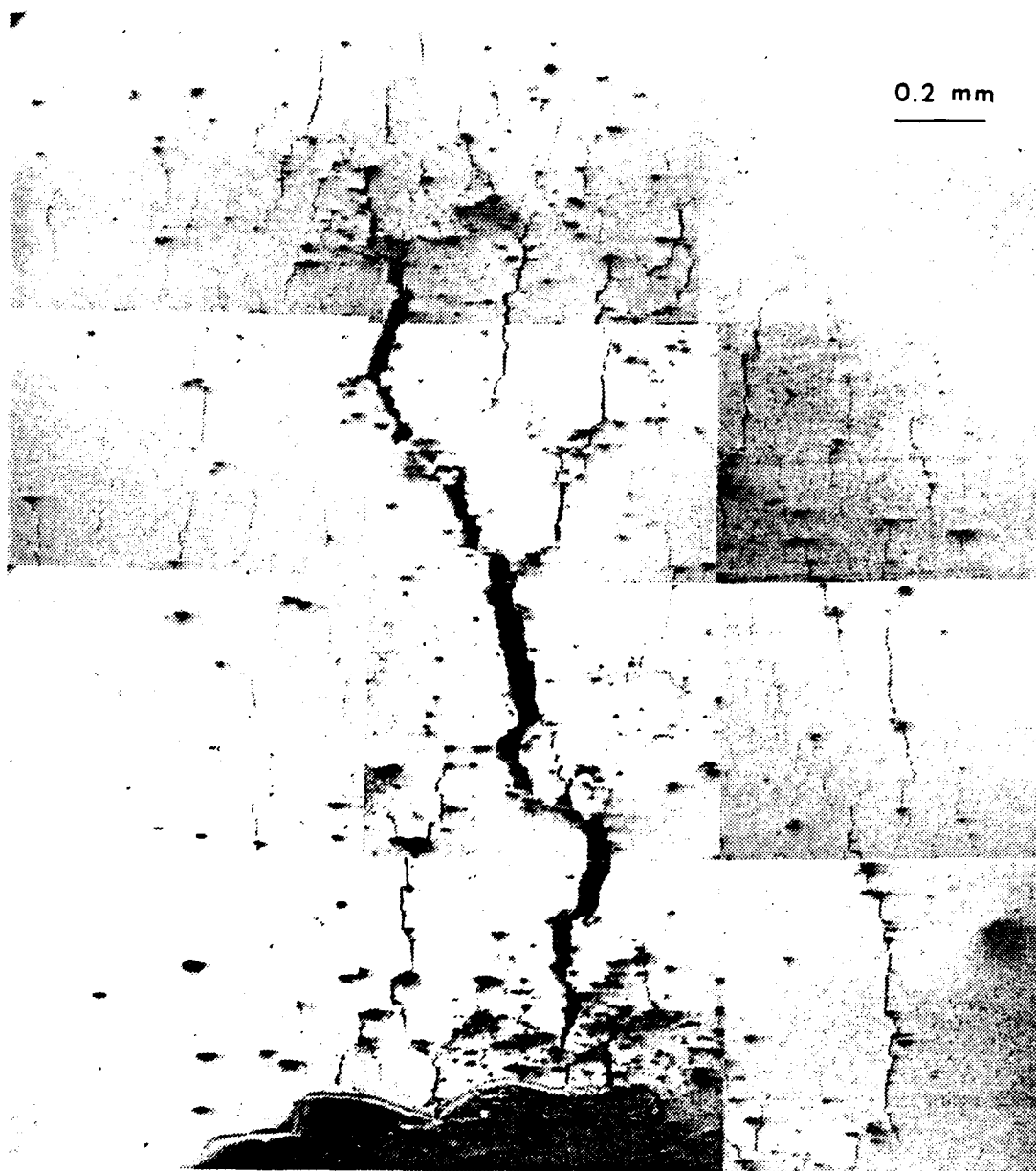
Figure A.23   Specimen #15   1430 Cycles.

69
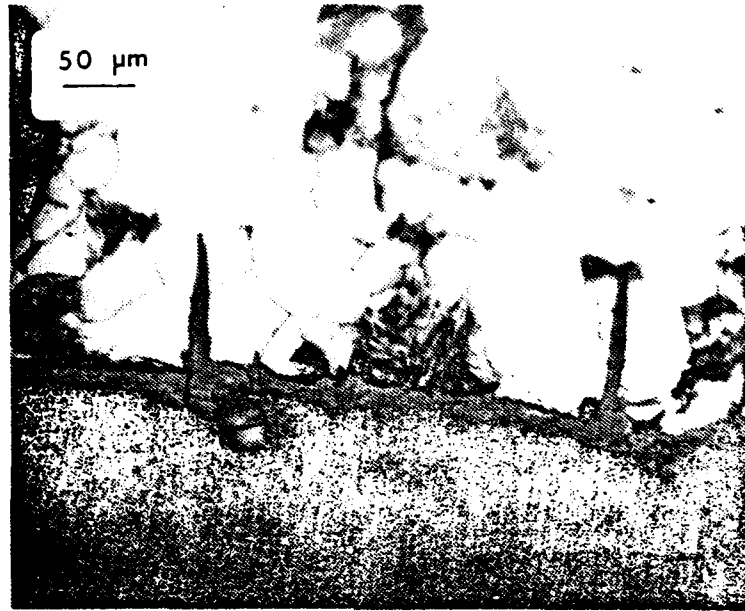
Figure A.24   Specimen #15   1430 Cycles.
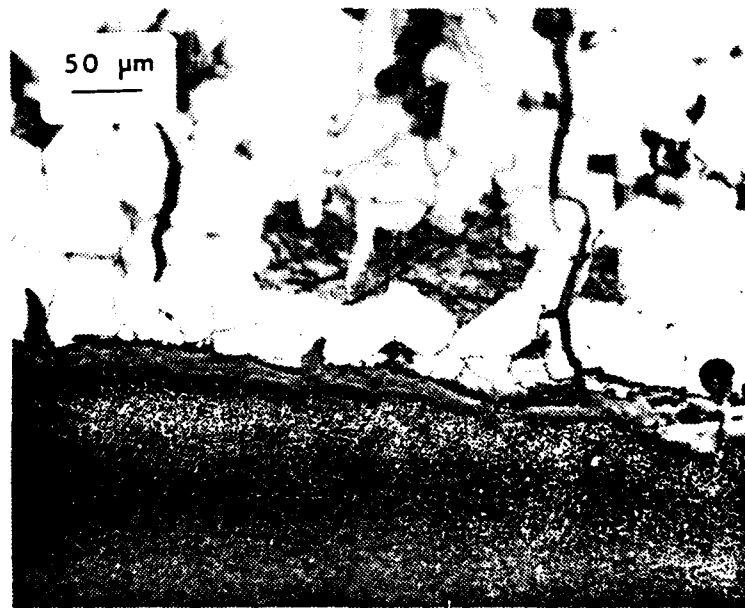
Figure A.25   Specimen #15   1430 Cycles.

50 µm
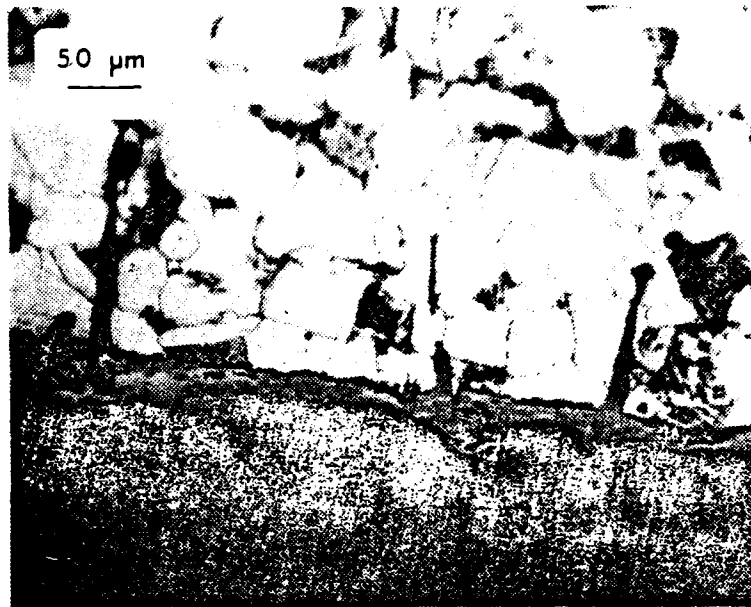
Figure A.26   Specimen #15   1430 Cycles.

50 µm
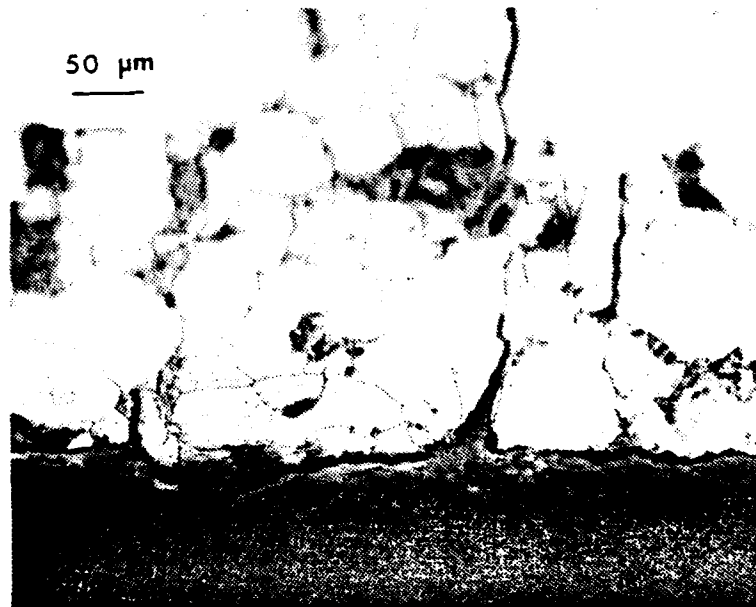
Figure A.27   Specimen #15   1430 Cycles.
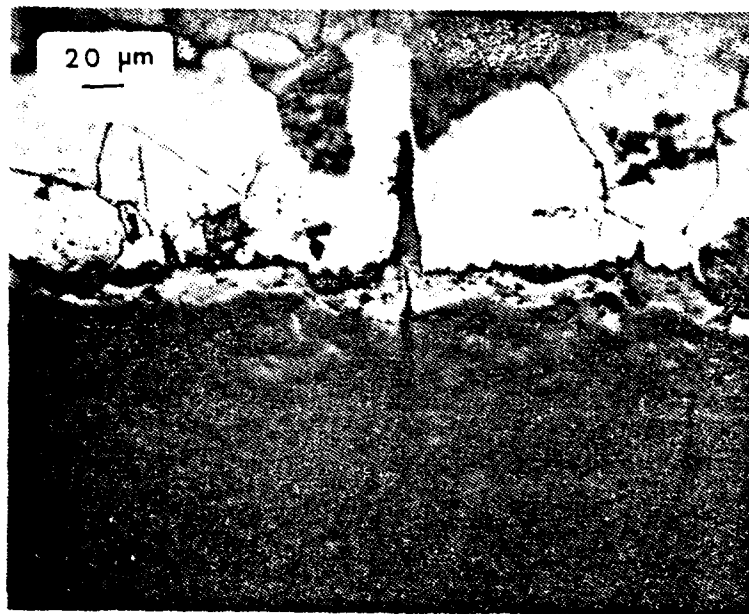
Figure A.28   Specimen #15   1430 Cycles.
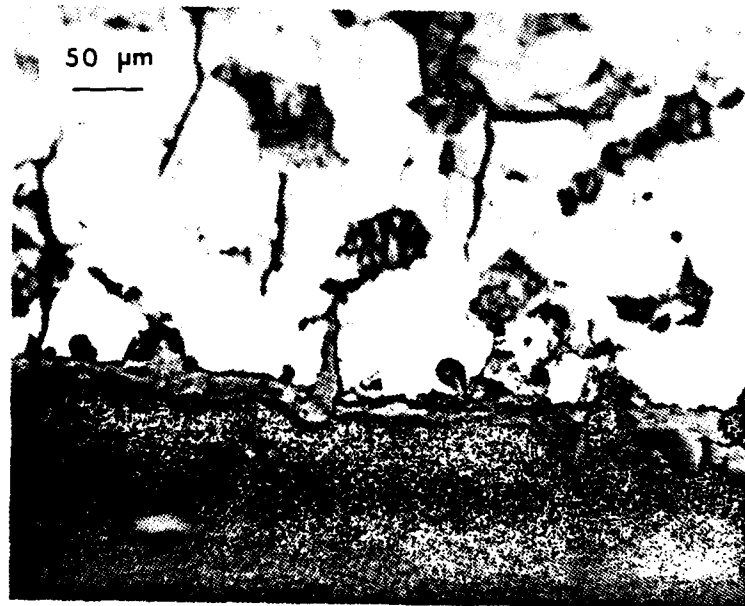
Figure A.29   Specimen #15   1430 Cycles.
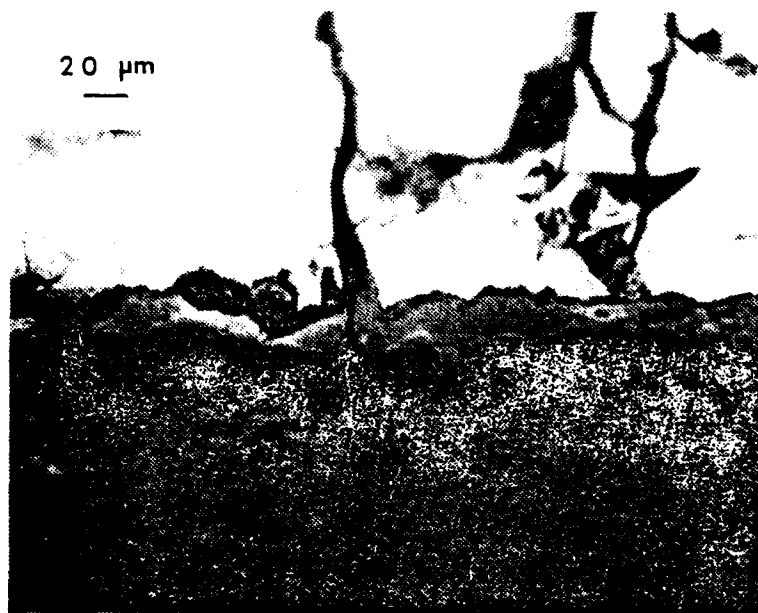
Figure A.30   Specimen #15   1430 Cycles.
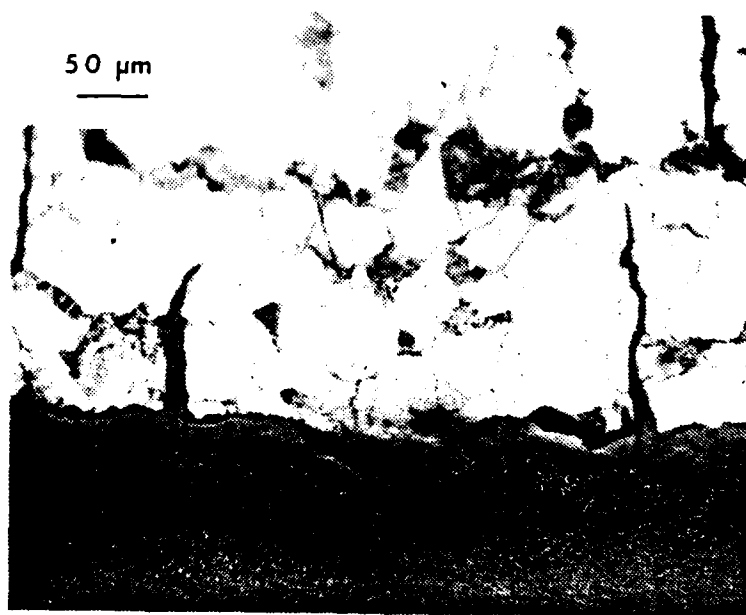
Figure A.31   Specimen #15   1430 Cycles.

73

20 μm
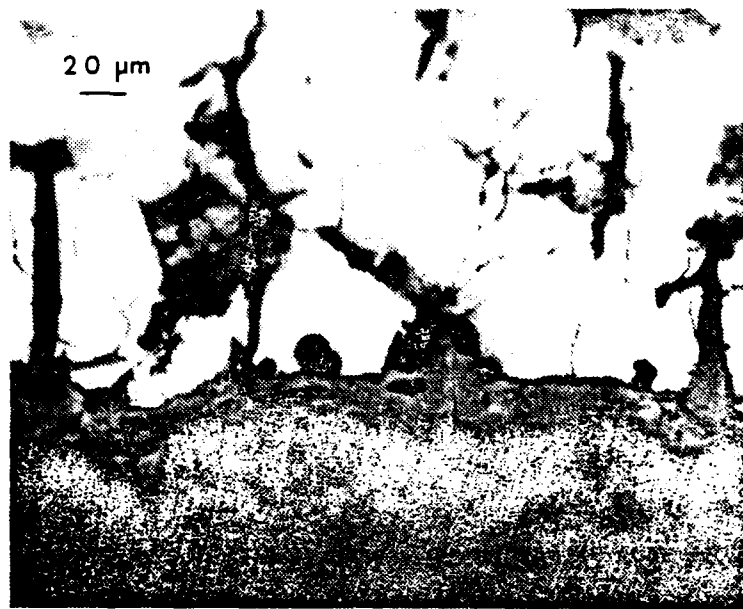
Figure A.32   Specimen #15   1430 Cycles.

20 μm

Figure A.33   Specimen #15   1430 Cycles.

Figure A.34   Specimen #15   1430 Cycles.

75

50 µm

Figure A.35   Specimen #15   1430 Cycles.
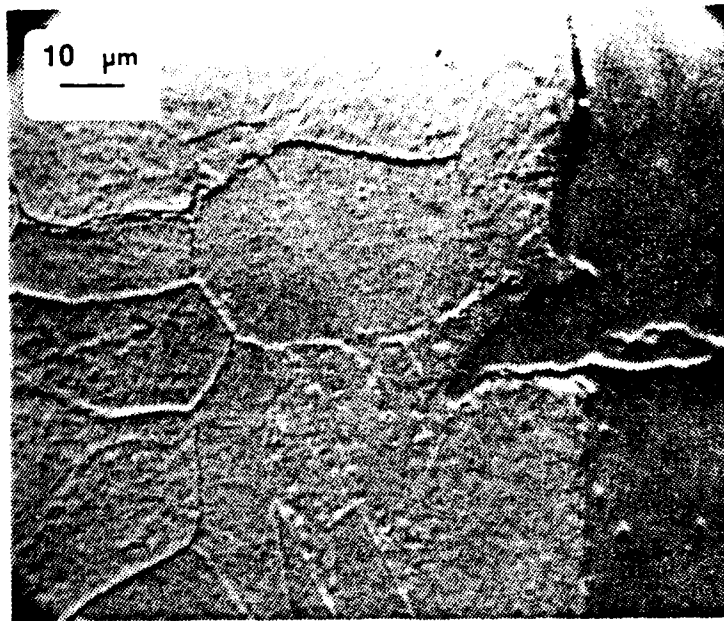
Figure A.36   Specimen #15   1430 Cycles.

Figure A.37   Specimen #15   1430 Cycles.

Figure A.38   Specimen #15   1430 Cycles.
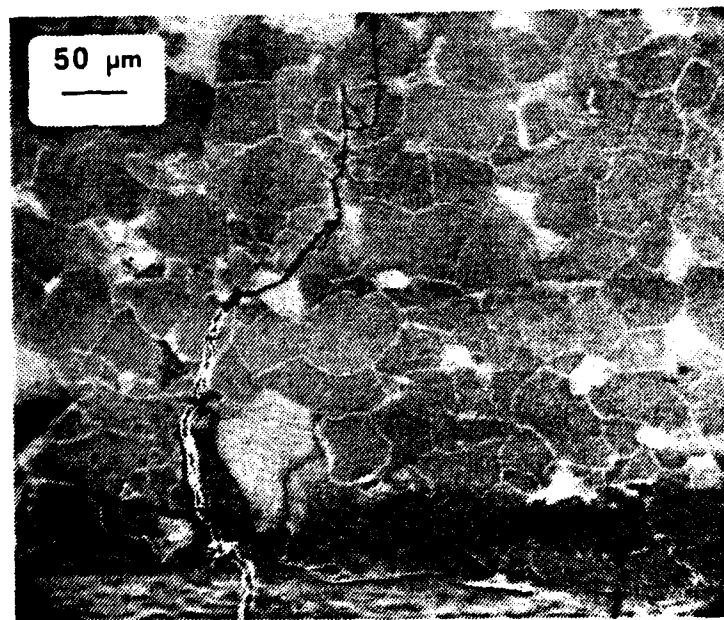
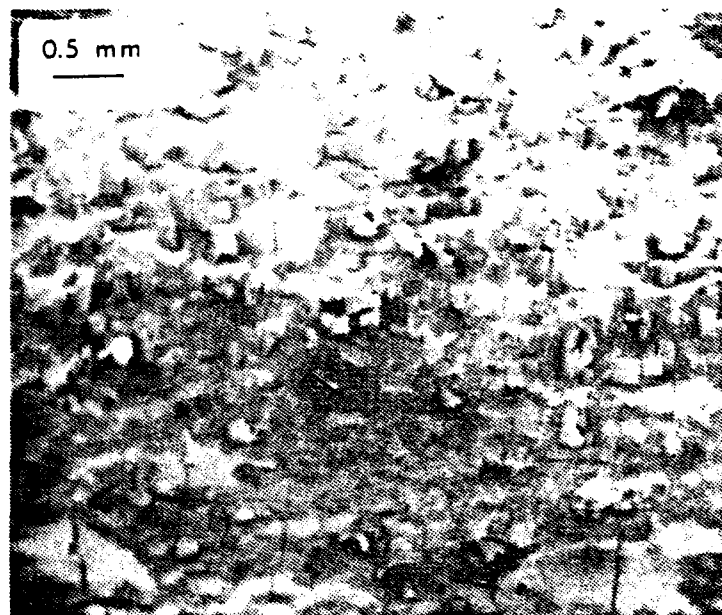Figure A.39   Specimen #15   1430 Cycles.

78
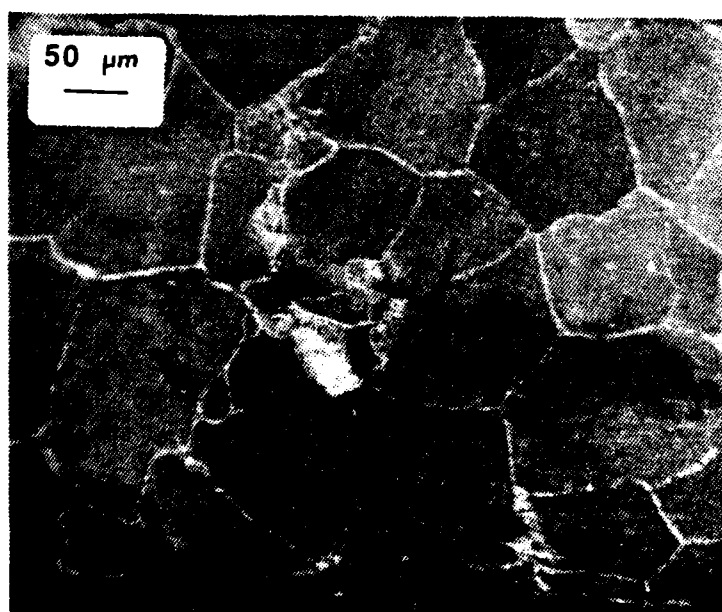
Figure A.40   Specimen #15   1430 Cycles.

Figure A.41   Specimen #15   1430 Cycles.

3. SPECIMEN #18   0.5% TOTAL STRAIN

Specimen #18 was cycled with a total strain range of 0.5%. The test was interrupted and the specimen examined on the SEM at 3153, 3300, 3450, 3600, 3750, and 3930 cycles. At 3153 cycles, most of the specimen surface was featureless, except one area which had some oxide cracking and spalling, Figure A.42. This area however did not become a site for fatigue cracking. At 3300 cycles, a small crack was detected, but its depth was not discernable, Figure A.43. This was considered the crack initiation point since at 3600 cycles, the crack had clearly propagated and penetrated the substrate. Figure A.44 shows the area at low magnification and Figure A.45 shows the crack tip at higher magnification. At 3750 cycles, continued propagation is evident in Figures A.46 and A.47. At 3930 cycles, continued growth and widening was observed as shown in Figures A.48 to A.51. Figure A.52 shows the same area after failure at 5322 cycles.

0.5 mm
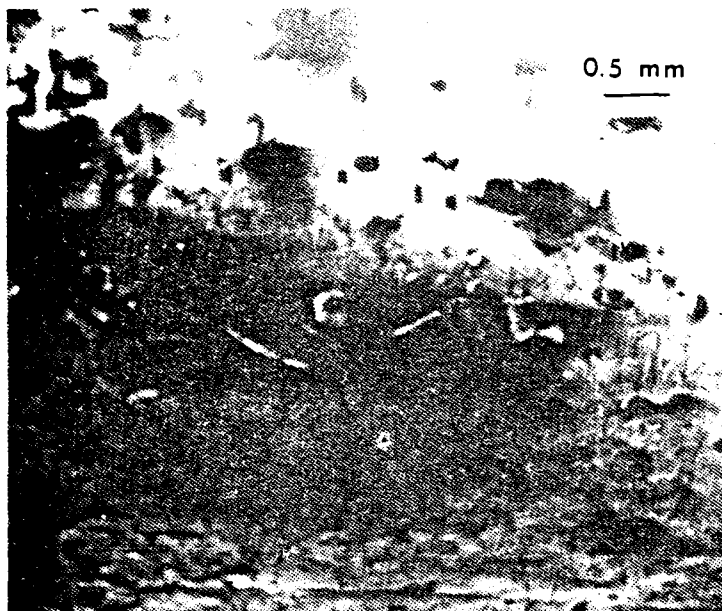
Figure A.42   Specimen #18   3153 Cycles.

10 μm
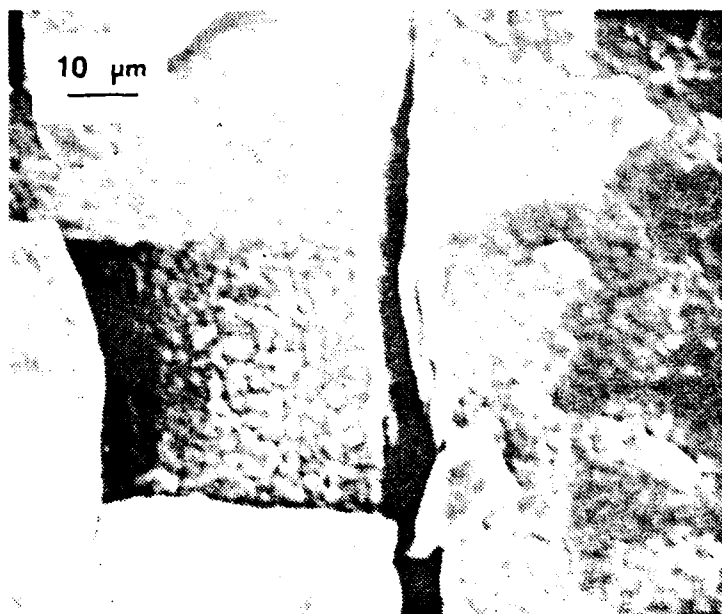
Figure A.43   Specimen #18   3300 Cycles.

82

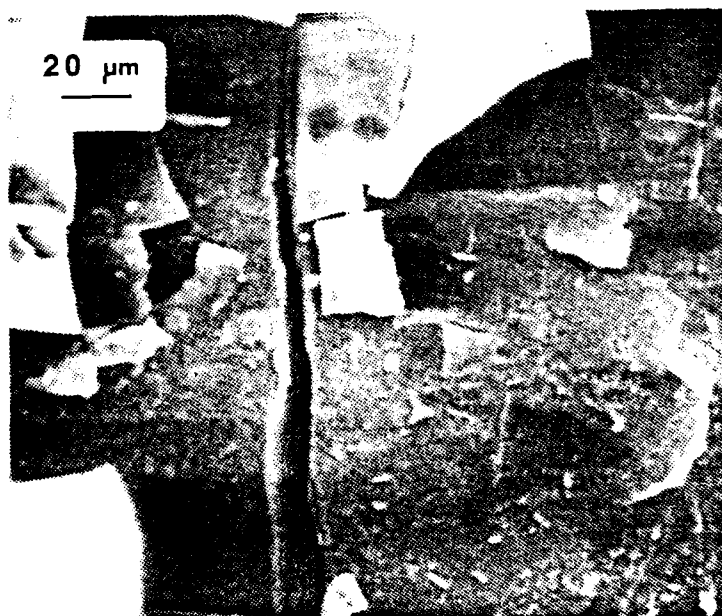Figure A.44   Specimen #18   3600 Cycles.

Figure A.45   Specimen #18   3600 Cycles.
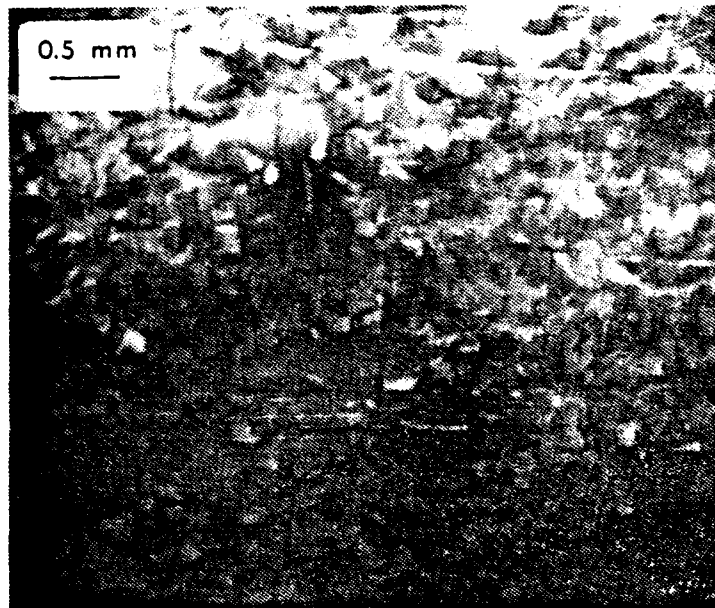
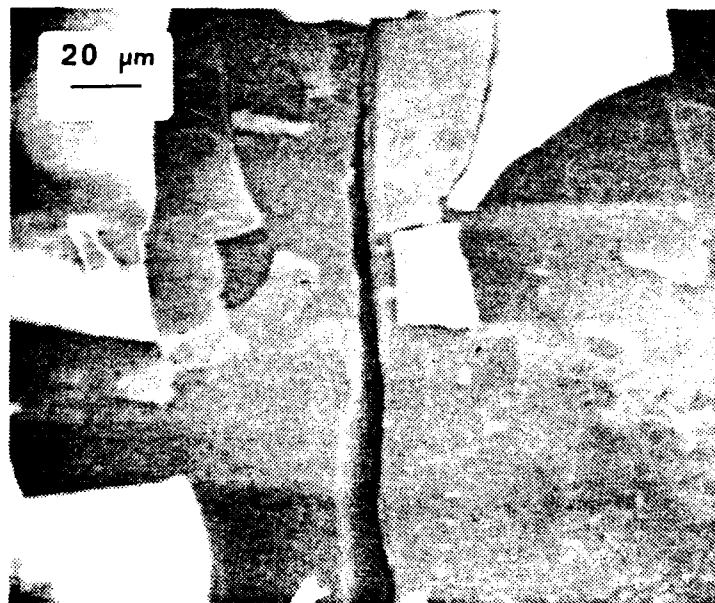Figure A.46   Specimen #18   3750 Cycles.

Figure A.47   Specimen #18   3750 Cycles.
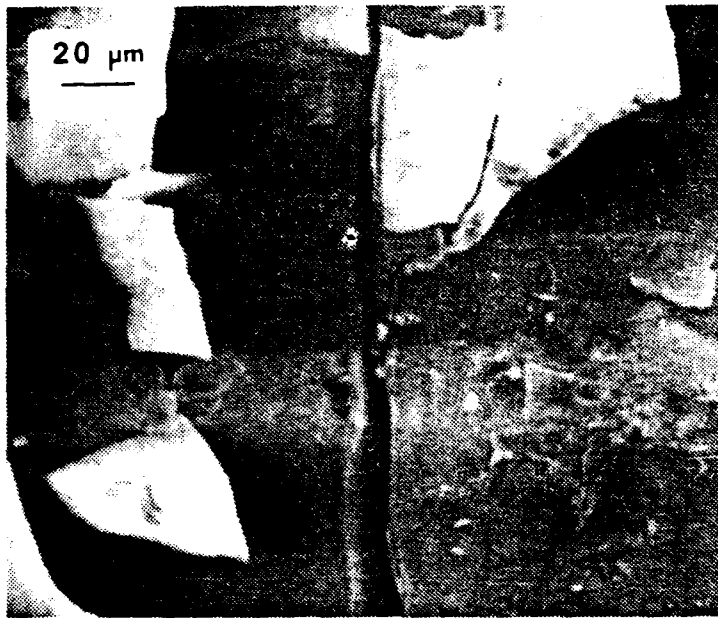
84

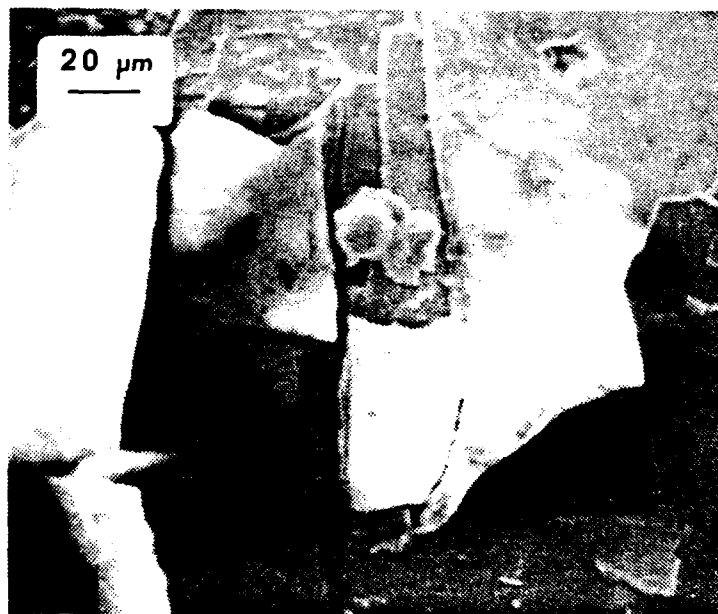Figure A.48   Specimen #18   3930 Cycles.

Figure A.49   Specimen #18   3930 Cycles.

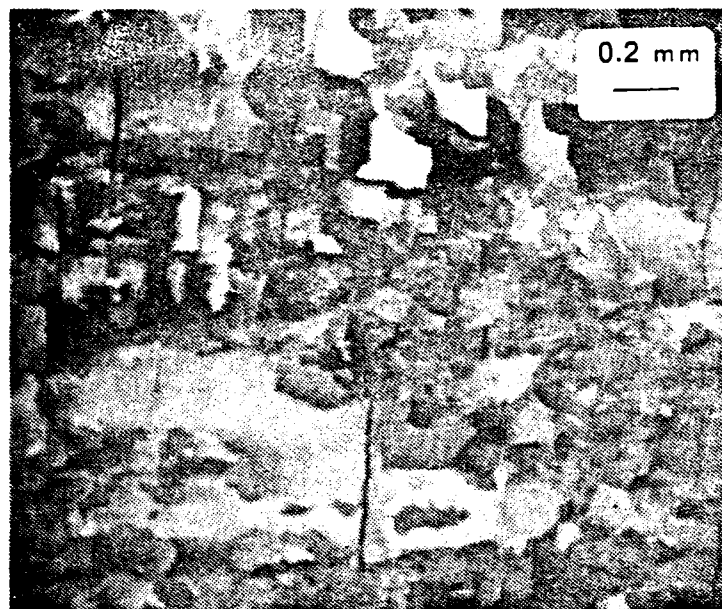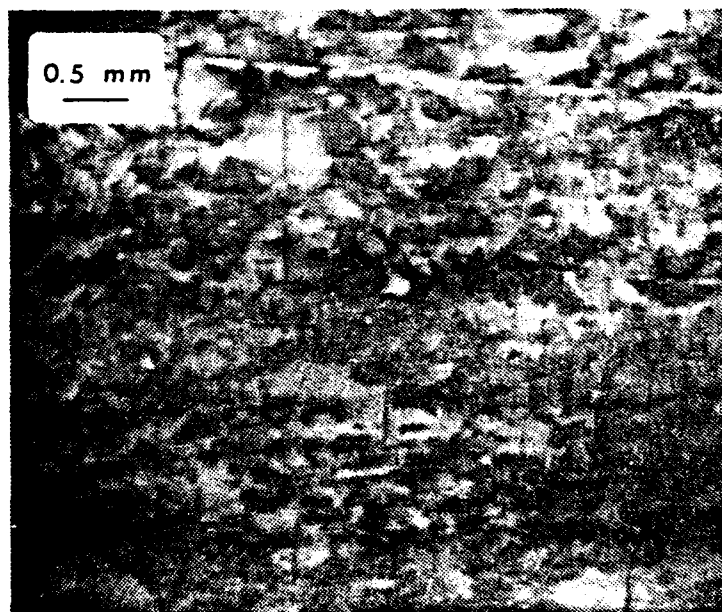Figure A.50   Specimen #18   3930 Cycles.

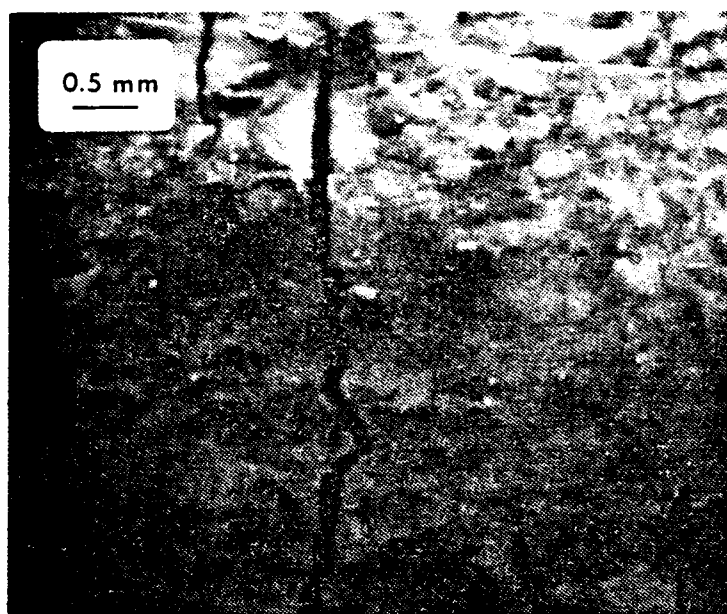Figure A.51   Specimen #18   3930 Cycles.

86

0.5 mm

Figure A.52   Specimen #18   5322 Cycles.

4. SPECIMEN #25 0.4% TOTAL STRAIN

Specimen #25 was continuously cycled at 0.4% total strain. The test was interrupted and the specimen examined at 6000, 7000, 8000, 8750, 9500, 1025, 11000, and 11750 cycles. At 6000 cycles, a defect in the oxide was visually noted consisting of a helical line running approximately 3/4 of the gage length and with approximately one rotation. Figure A.53 shows one portion of this line. This is believed to be caused by the machining of the gage length and it did not show any signs of cracking throughout the specimen's life. In addition, one area showed oxide defects which seem to correspond to grain boundaries, Figures A.54 and A.55. This area was monitored and later in life was the crack initiation site. At 10250 cycles, this area showed little change at low magnification, as shown in Figures A.56 and A.57. At 11750, this area had several cracks, Figures A.58 and A.59. Examination at higher magnification revealed a large crack extending over a 60° arc, Figures A.60 and A.61, indicating that the crack had been propagating over several of the previous examinations. A calculation was made to extrapolate the initiation point. Crack growth was monitored in specimen #31, cycled with 1% total strain. Approximately 75% of the cycles to propagate the crack to failure were required to propagate the crack to a 60° arc length. Using the same proportion, would indicate that the crack initiated at about 9900 cycles. This estimate is supported by two other observations. First, fatigue propagation occurred over 2022 cycles in specimen #18 cycled at 0.5% total strain. It is reasonable to assume that crack propagation in this sample would require at least as many cycles, and probably more. Second, at 10250 cycles, a spalled area is visible on the lower portion of Figure A.57. This corresponds to the spalled portion of Figure A.59,

indicating that the crack was probably present at 10250 cycles, but not observed. The specimen was then cycled without interruption to failure which occurred at 12376 cycles.
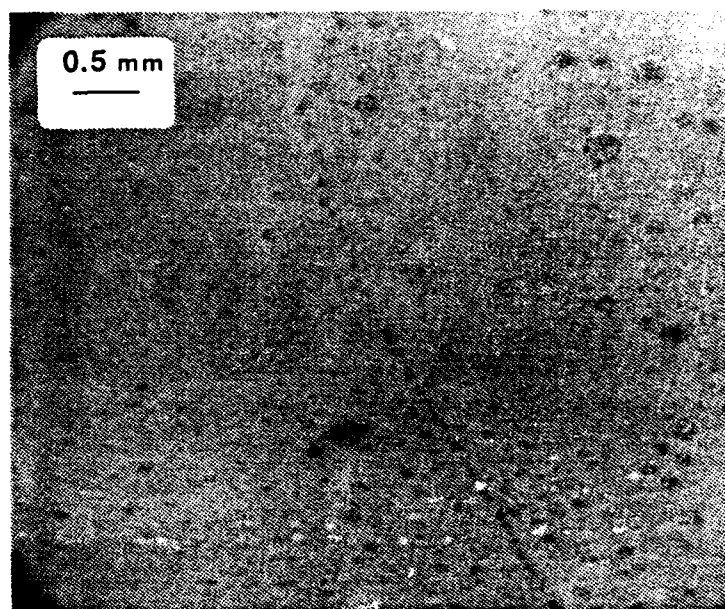

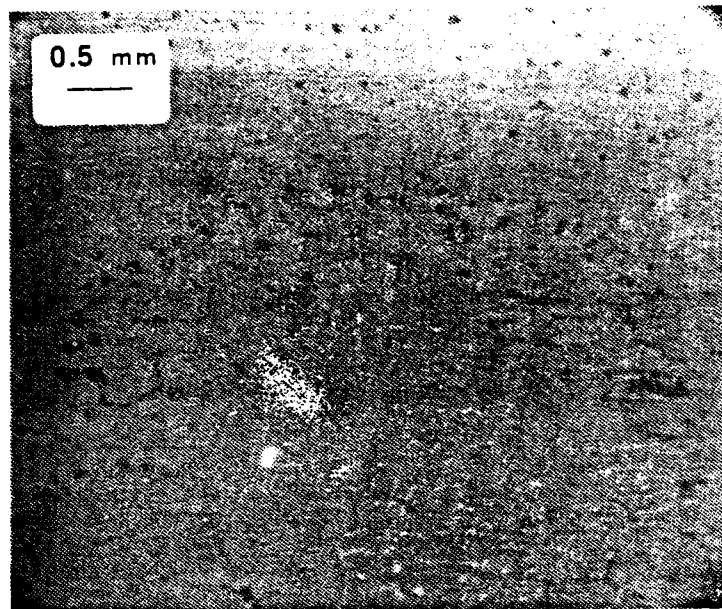Figure A.53   Specimen #25   6000 Cycles.
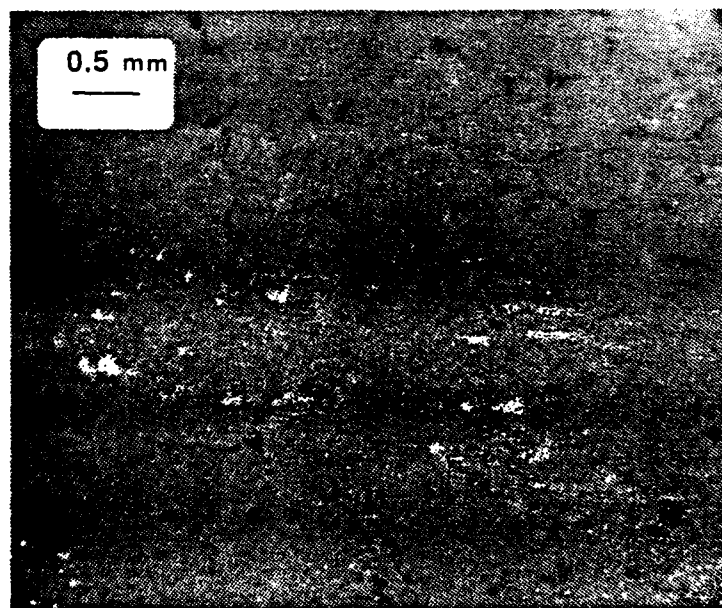
0.5 mm

Figure A.54   Specimen #25   6000 Cycles.

0.5 mm

Figure A.55   Specimen #25   6000 Cycles.

0.5 mm

Figure A.56   Specimen #25   10250 Cycles.

0.5 mm

Figure A.57   Specimen #25   10250 Cycles.

91

0.5 mm

Figure A.58   Specimen #25   11750 Cycles.
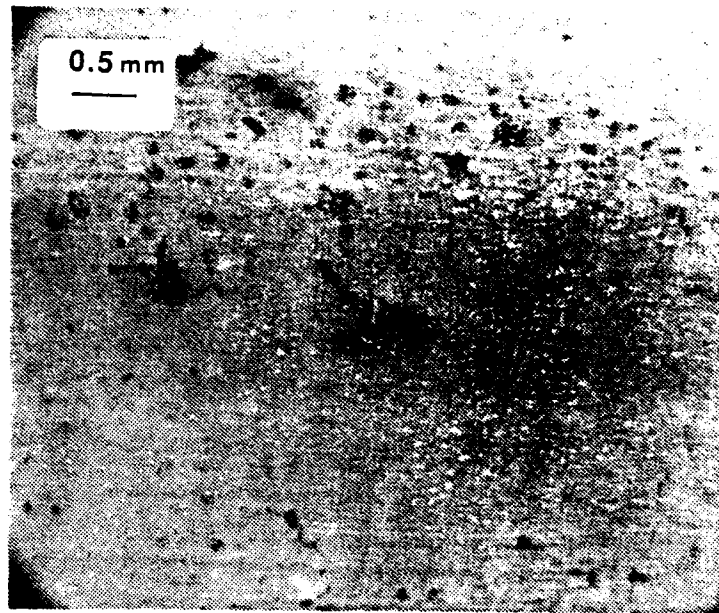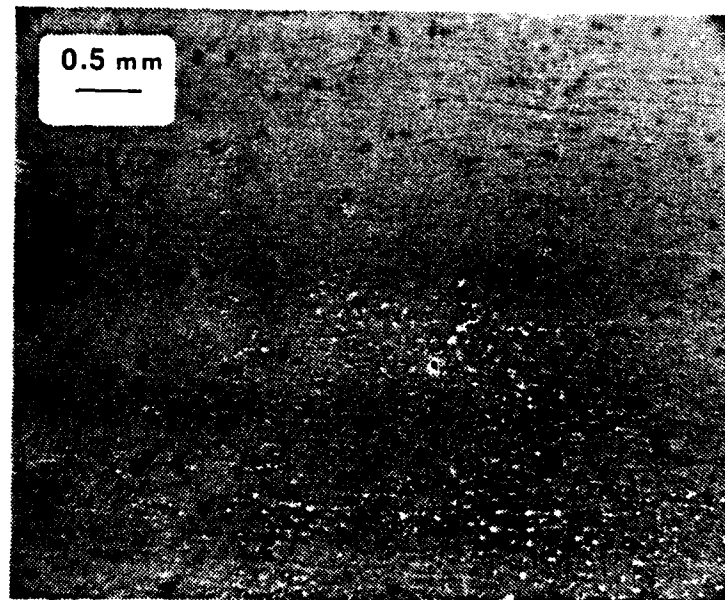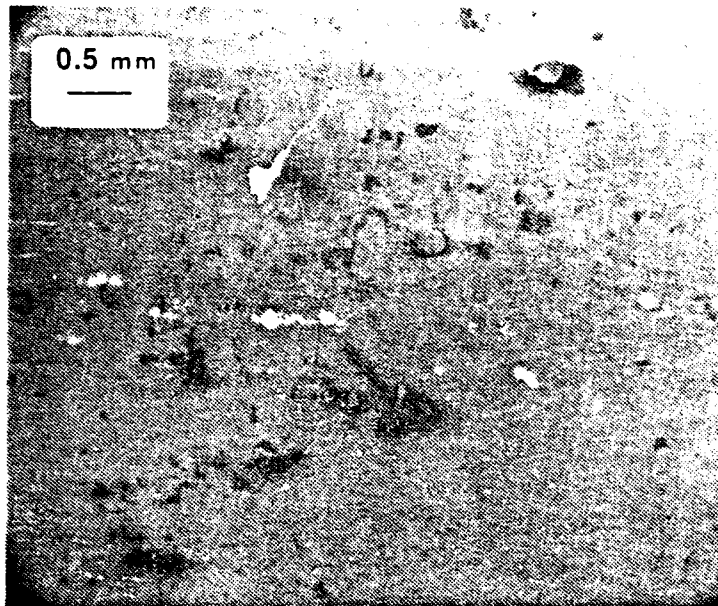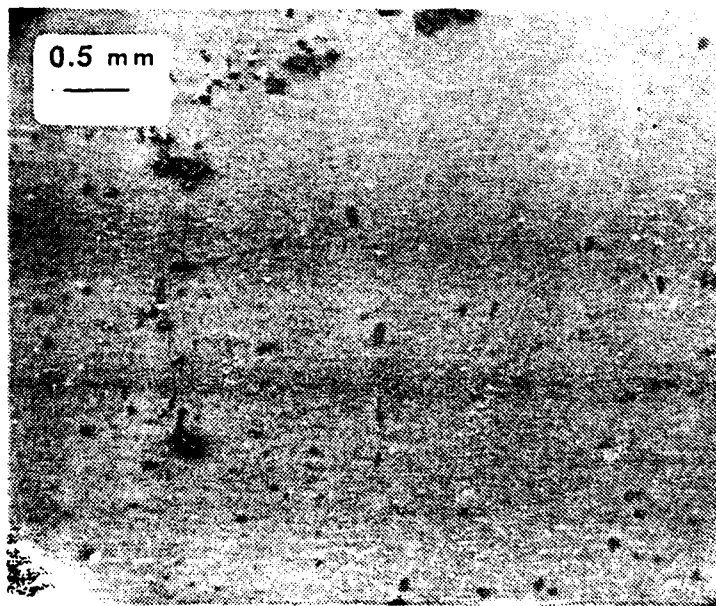

0.5 mm

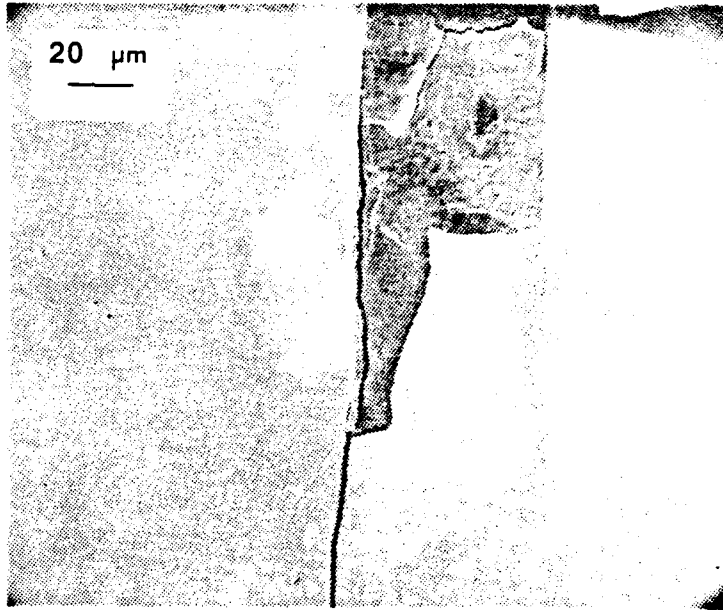Figure A.59   Specimen #25   11750 Cycles.

Figure A.60   Specimen #25   11750 Cycles.
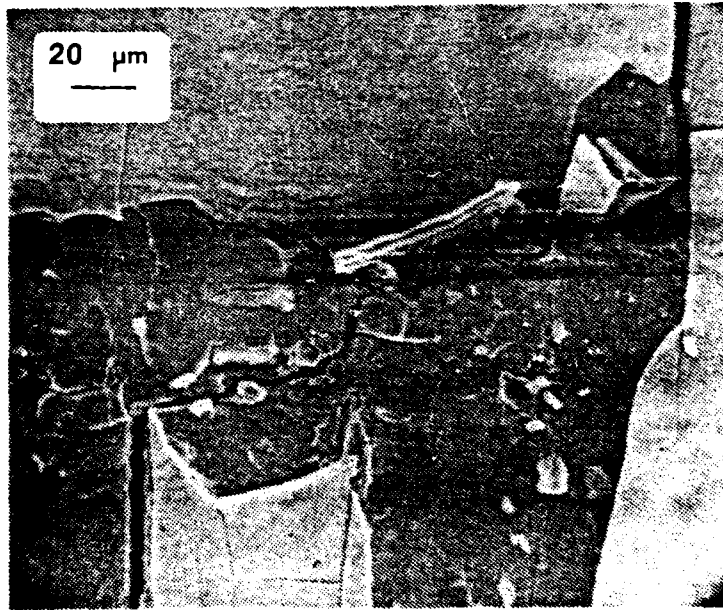

Figure A.61   Specimen #25   11750 Cycles.

93

5. SPECIMEN #24   0.35% TOTAL STRAIN RANGE

Specimen #24 was cycled with a total strain range of 0.35%. Testing was interrupted and the specimen examined on the SEM at 22750, 25500, 27222, 29236, 32000, and 34634 cycles. At 22750 cycles, the oxide layer showed one area of cracking, however no penetration of the substrate was noted, Figure A.62. At 25500 cycles no change was noted. At 27222 cycles, the upper button head of the specimen failed due to a fatigue crack which initiated at the button head fillet. A thread was machined onto the specimen shank and a thread type grip was used for further testing. No change was noted on the surface of the specimen upon examination at 27222 cycles. At 29236 cycles, the lower button head failed for the same reason, and a thread was machined in the specimen shank as before. Examination of the specimen at 29236 cycles showed that the oxide remained intact despite the thermal transients associated with the button head failures. Additionally, the oxide crack noted previously appeared to grow but no penetration into the substrate could be confirmed, Figures A.63 and A.64. By 32000 cycles, the crack had both grown, and widened, Figures A.65 to A.67, and had penetrated the substrate, indicating that the crack initiated at about 29236 cycles. At 34634 cycles, fatigue failure occurred on the upper screw on the specimen shank, and no further testing could be conducted, giving a lower bound to the number of cycles to failure of this specimen. The specimen was then examined and the crack had clearly propagated, Figures A.68 and A.69. For this thesis, it is useful to extrapolate the failure point using the crack growth information derived from specimen #31. Approximately 53% of the propagation life was required to propagate a

94

crack in specimen #31 to a comparable length as those in this specimen at 34634 cycles. Using the same proportion, failure should have occurred at about 39300 cycles. This gives a best estimate for comparison with the other data.
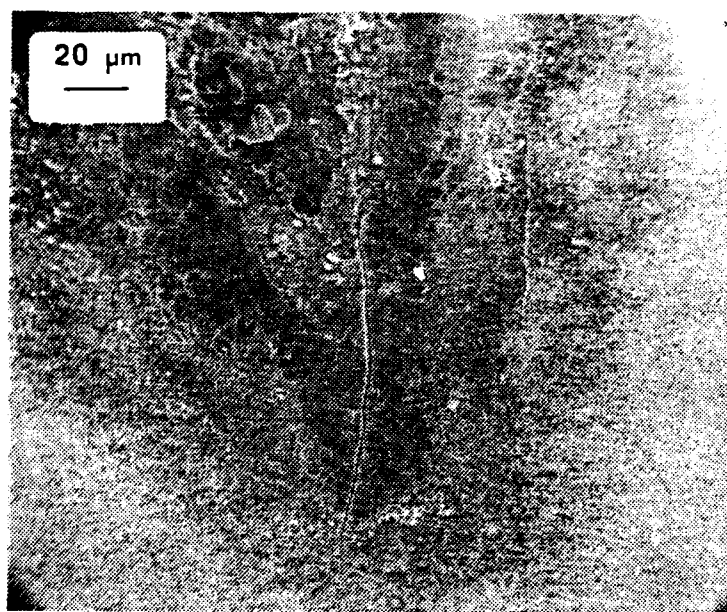

Figure A.62   Specimen #24   22750 Cycles.

END

FILMED

DTIC
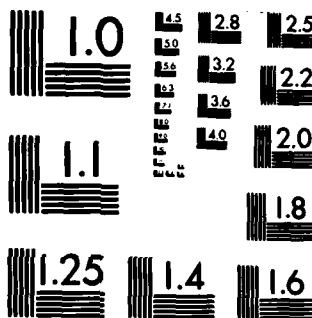
MICROCOPY RESOLUTION TEST CHART

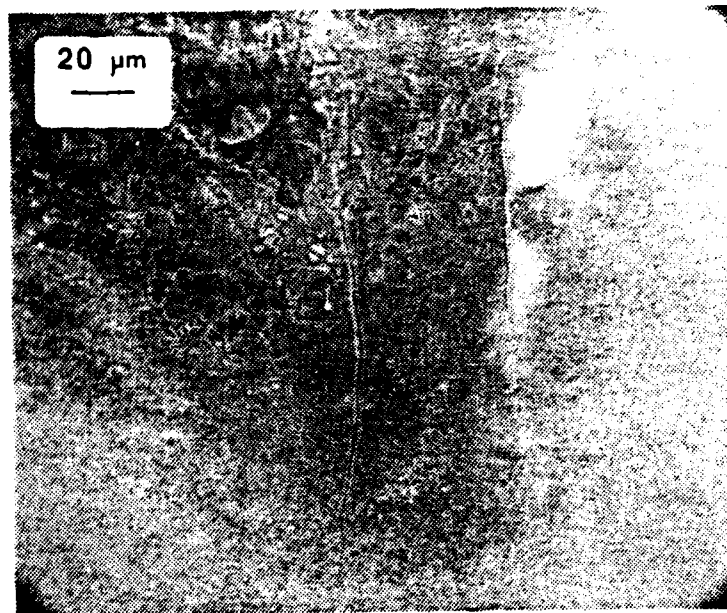NATIONAL BUREAU OF STANDARDS-1963-A

Figure A.63   Specimen #24   29236 Cycles.
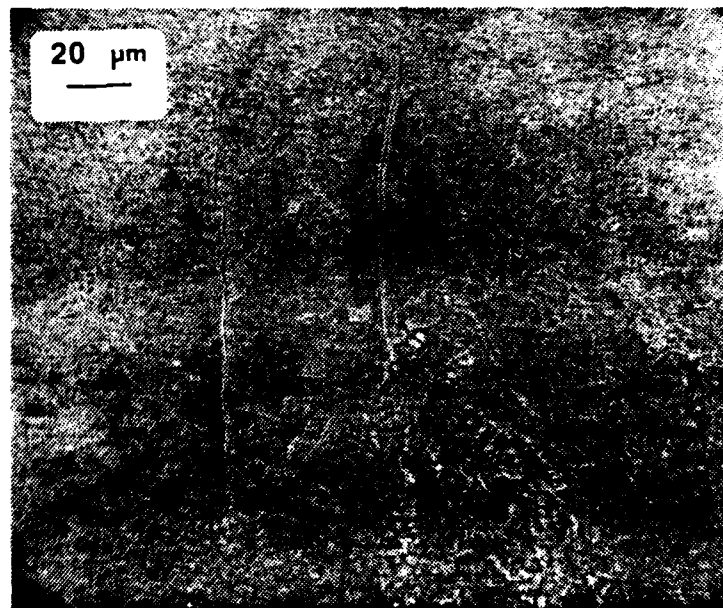

Figure A.64   Specimen #24   29236 Cycles.
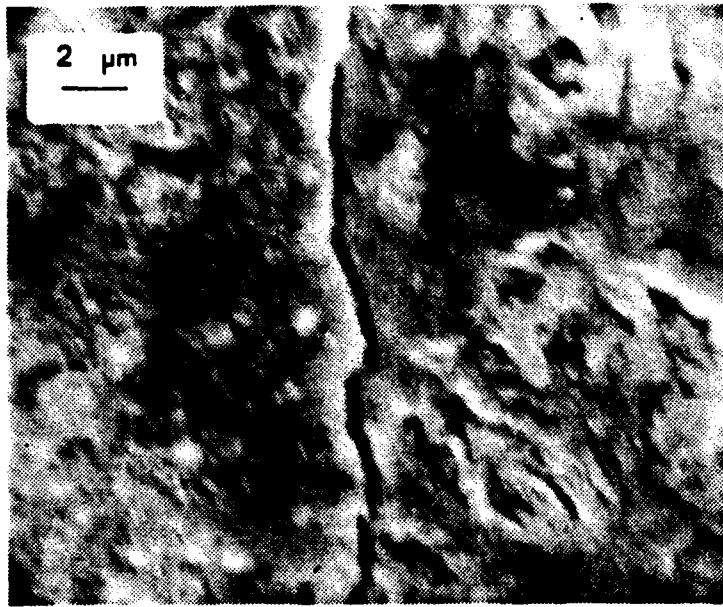
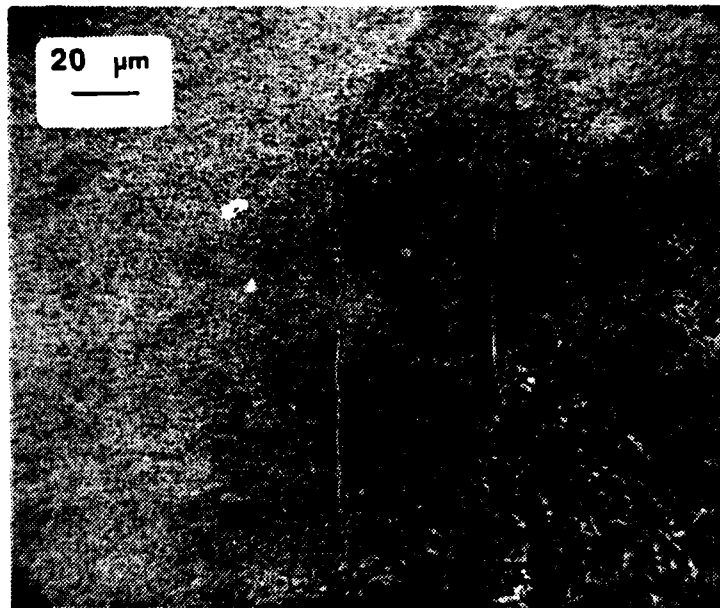Figure A.65   Specimen #24   32000 Cycles.

Figure A.66   Specimen #24   32000 Cycles.
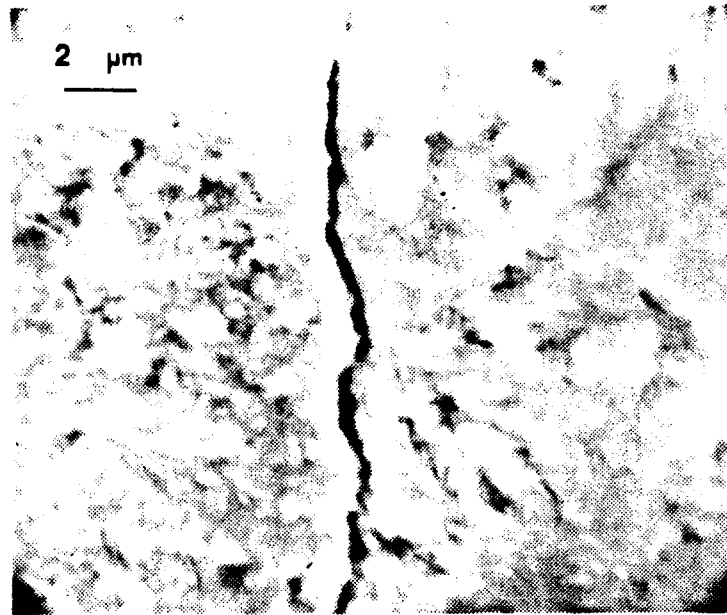
97

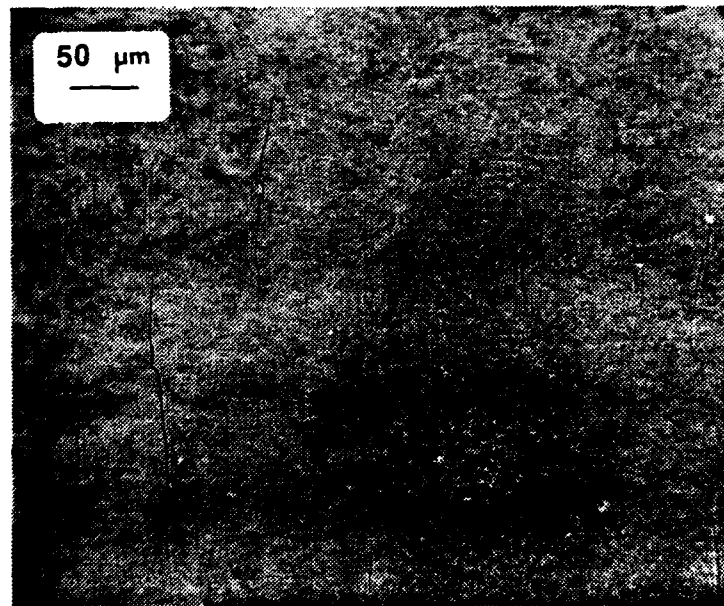Figure A.67   Specimen #24   32000 Cycles.

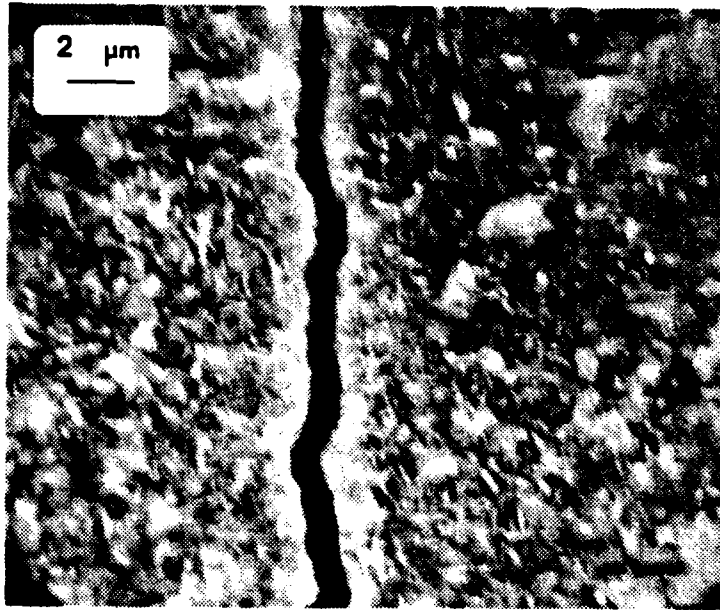

Figure A.68   Specimen #24   34634 Cycles.

98

Figure A.69   Specimen #24   34634 Cycles.

6. SPECIMEN #14 0.3% TOTAL STRAIN

Specimen #14 was cycled at 0.3% total strain range. The test was interrupted and the specimen examined on the SEM at 30000, 33000, 36300, 39900, 43900, 48410, 53200, 55950, 70800, 76330, 79779, and 79908 cycles. This sample was plagued with problems and was not cycled to failure. The cycling progressed normally until 76330 cycles, at which time the upper button head failed due to a fatigue crack initiated by the button head fillet. This caused the MTS system and induction heater to trip, and resulted in rapid cool down of the specimen. There was some increased cracking of the oxide but the oxide was generally intact. A thread end was machined on the upper specimen shank which allowed reinsertion of the specimen with a threaded grip. When the specimen was examined on the SEM, no fatigue cracks were evident. At 79908 cycles, the specimen formed a small neck presumably due to the extensometer slipping. Rapid operator action minimized the cool down, however the oxide layer spalled off. The specimen was reinserted and cycling began again, since the strain range was small and the neck was outside the extensometer monitoring length. At 79,908 cycles, the specimen started to buckle and the cycling was stopped. Subsequent examination showed no cracking or even any potential initiation points. This indicates a lower bound on the number of cycles to crack initiation at 0.3% total strain range, and is included since an additional data point at 0.3% strain was impossible to run.

7. SPECIMEN #32 0.5% TOTAL STRAIN WITH COMPRESSIVE DWELL

Specimen #32 was cycled with a total strain range of 0.5% and a 5 minute dwell on each cycle at the maximum compressive strain. The test was interrupted and the specimen examined at 300 and 595 cycles. At 300 cycles, intense circumferential oxide cracks were visible to the unaided eye in the top 1/3 of the specimen gage length. This observation was confirmed on the SEM, Figure A.70. Oxide cracking was also observed throughout the gage length, but was less intense on the lower 2/3, Figure A.71. Examination at higher magnification showed penetration of the substrate, Figures A.72 and A.73, indicating that crack initiation occurred at less than 300 cycles. At 595 cycles, many of the cracks had widened and deepened while others seemed to seal with oxide, as shown in comparing Figures A.70 and A.74. Figures A.75, A.76, and A.77 clearly show cracking of the substrate. The specimen was then cycled to failure, with visual monitoring. At 750 cycles, three areas showed spalling of the oxide layer, with increased spalling as the test progressed. Failure of the specimen occurred at 1949 cycles.

Examination of the fracture surface showed that the fatigue crack initiated on numerous points on the surface of the specimen. These individual cracks grew to form a single crack which was convexed toward the specimen surface, which is typical of a fatigue initiated by a circumferential groove, Figure A.78. All specimens cycled without dwell had a single crack initiation site and the crack front was concaved toward the origin. This clearly shows that oxide cracks must initiate the cracks in the substrate, since the compressive dwell's initial affect is to promote profuse circumferential oxide cracks.
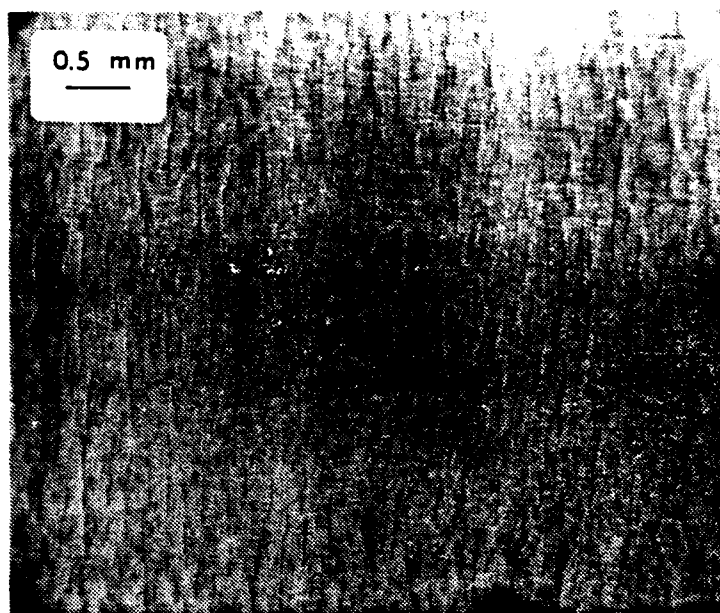
Figure A.70   Specimen #32   300 Cycles.

Figure A.71   Specimen #32   300 Cycles.

2 μm

Figure A.72   Specimen #32   300 Cycles.
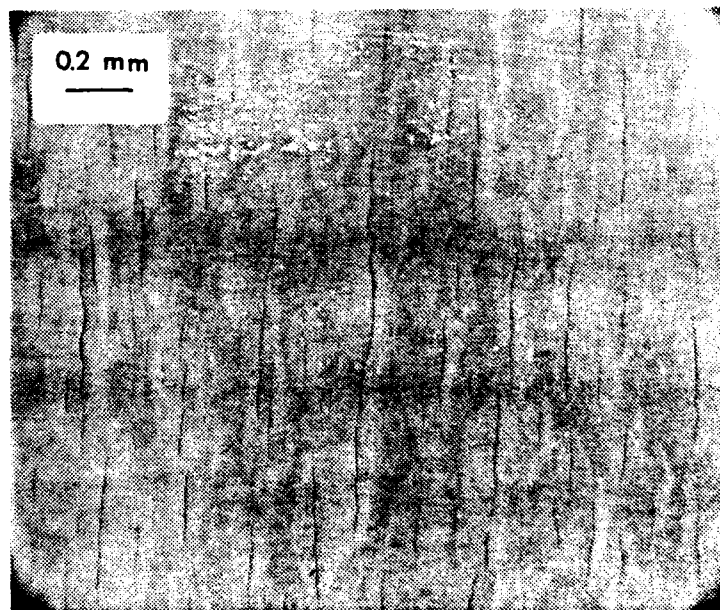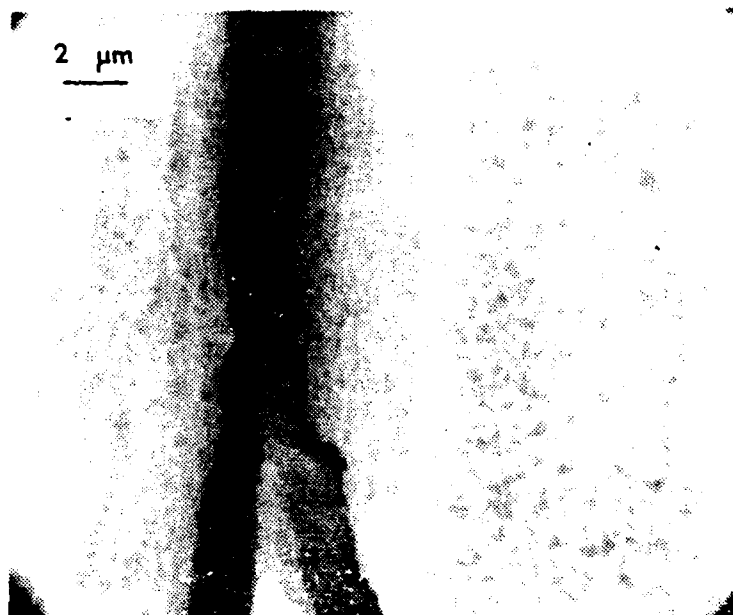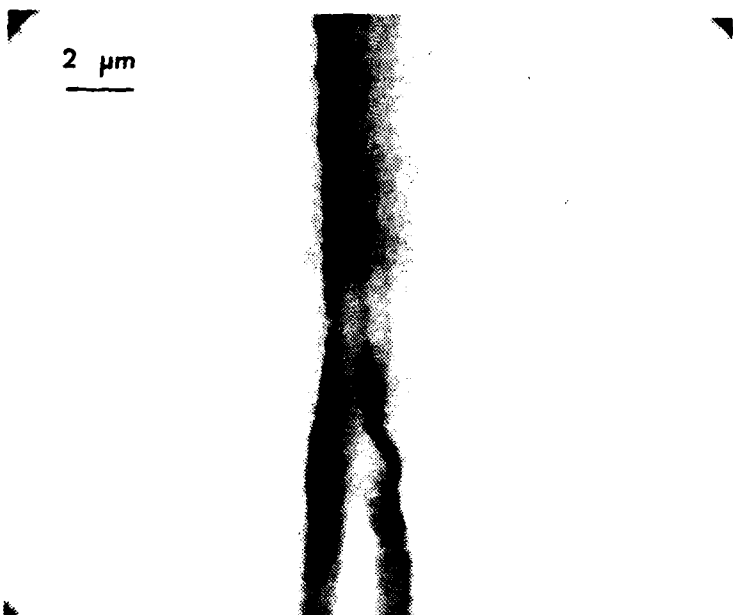

2 μm

Figure A.73   Specimen #32   300 Cycles.
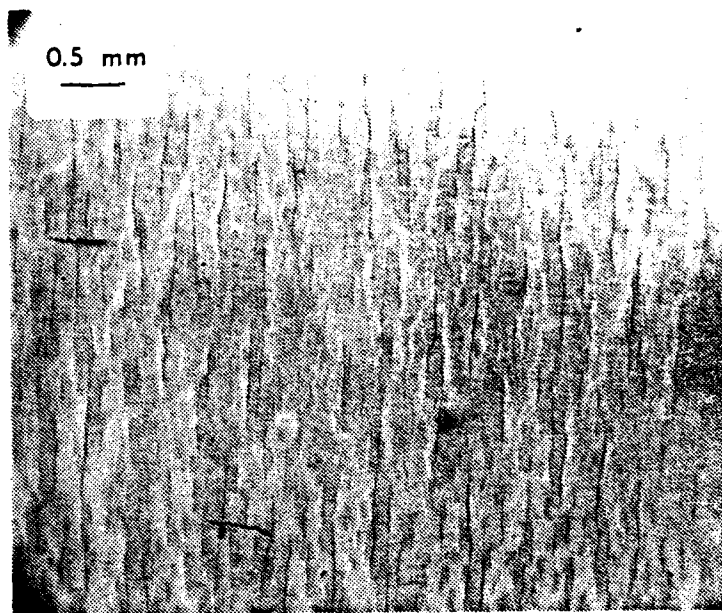
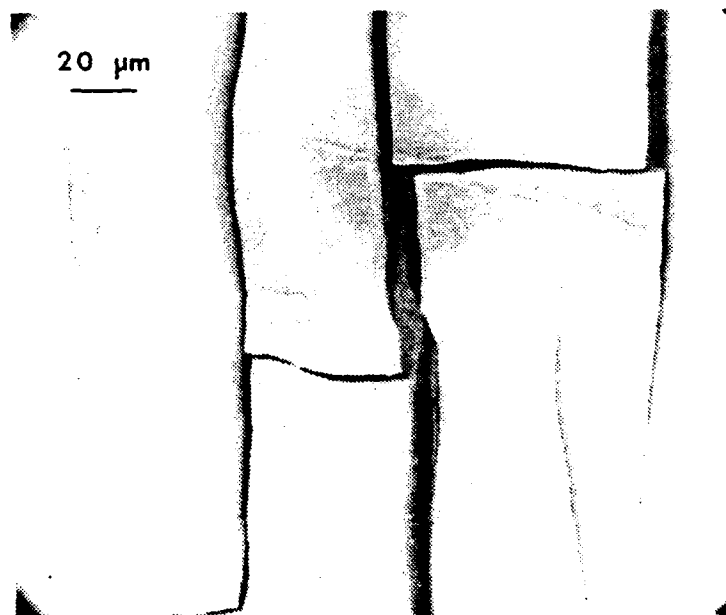Figure A.74   Specimen #32   595 Cycles.

Figure A.75   Specimen #32   595 Cycles.
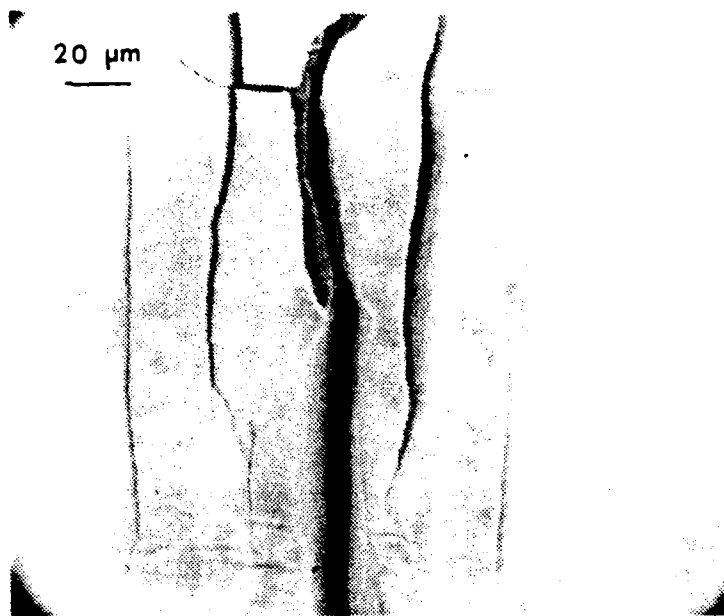
104

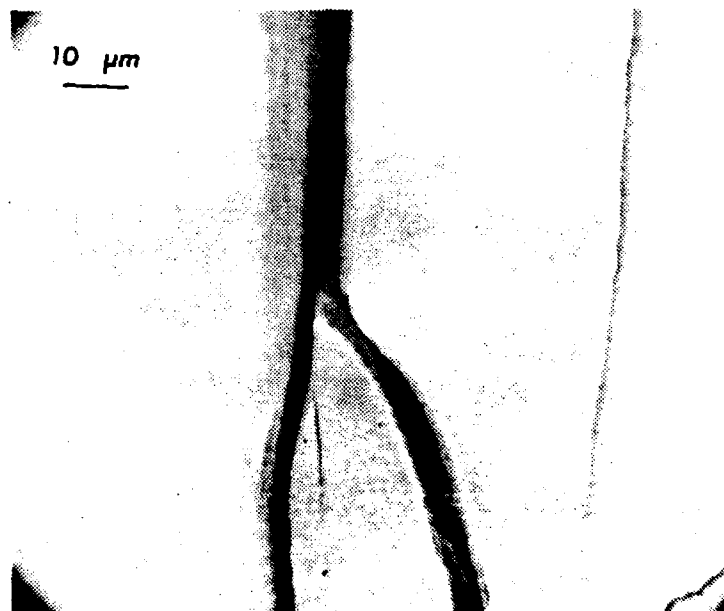Figure A.76   Specimen #32   595 Cycles.
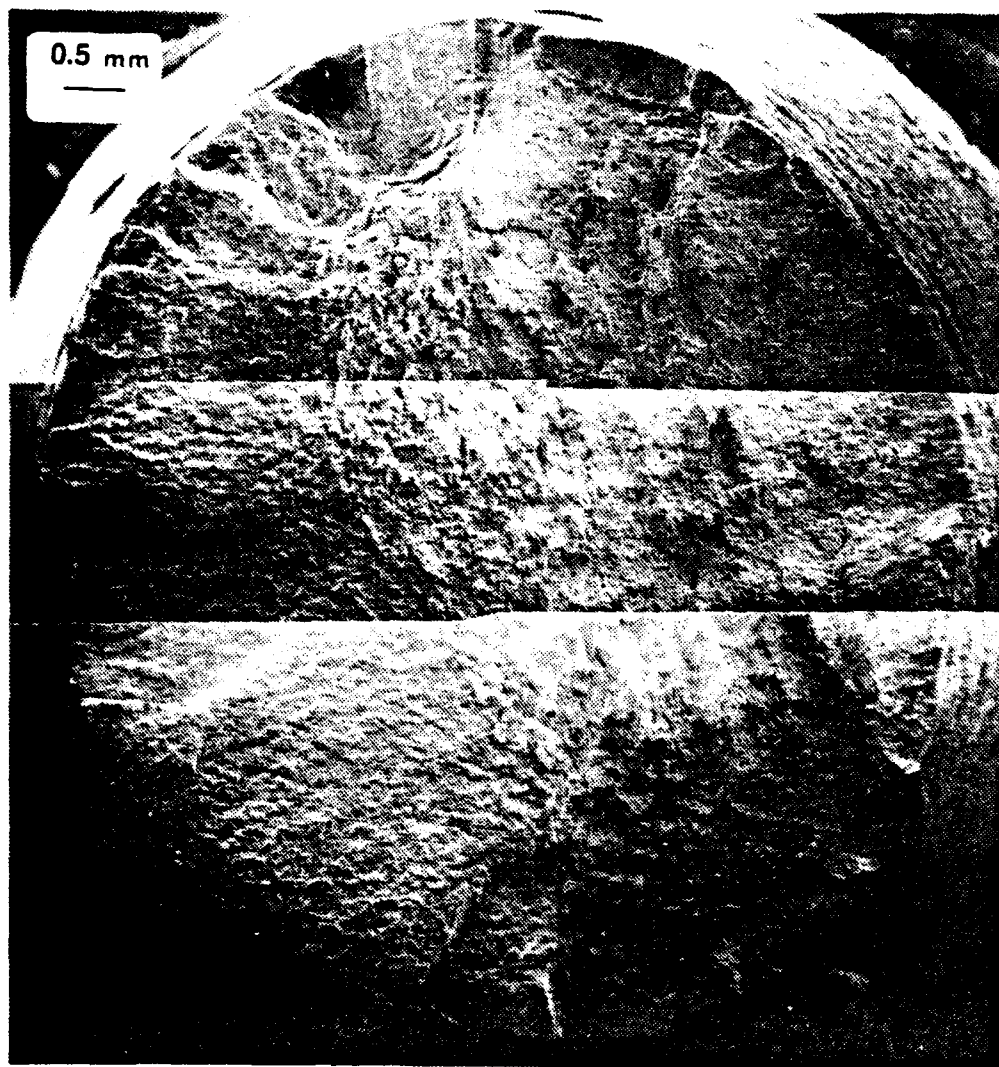

Figure A.77   Specimen #32   595 Cycles.

105

Figure A.78   Specimen #32 Fracture Surface.

LIST OF REFERENCES

1. Challenger, K. D., "Elevated Temperature Fatigue of 2 1/4 Cr- 1 Mo Steel", paper to be presented to the 6th International Conference on Fracture, New Delhi, India, December 1984.

2. Brinkman, C. R., _Fatigue, Environmental and Temperature Effects_, Plenum Press, New York, p. 247, 1980.

3. Skelton, R. P., and Bucklow, J. I., "Cyclic Oxidation and Crack Growth during High Strain Fatigue of Low Alloy Steel", _Metal Science_, Vol. 12, p. 64, 1978.

4. Chopra, O. K., Natesau, K., and Kassner, T. F., paper presented to the 2nd International Conference on Liquid Metal Technology in Energy Production, Richland, Washingtion, 1980.

5. Haigh, J. R., Skelton, R. P., and Richards, C. E., "Oxidation-assisted Crack Growth during High Cycle Fatigue of a 1% Cr-Mo-V Steel at 550 °C", _Material Science and Engineering_, Vol. 26, pp. 167-174, 1976.

6. Challenger, K. D., Miller, A. K., and Brinkman, C. R., "An Explination for the Effects of Hold Periods on the Elevated Temperature Fatigue Behavior of 2 1/4 Cr - 1 Mo Steel" _Journal of Engineering Material Technology_, Vol. 103, pp. 7-14, January 1981.

7. Challenger, K. D., Miller, A. K., and Langdon, R. I., "Elevated Temperature Fatigue with Hold Time in a Low Alloy Steel: A Predictive Correlation" _Journal of Material Energy Systems_, Vol. 3, pp. 51-61, June, 1981.

8. White, D. J., "Effect of Environmental hold time on the High Strain Fatigue Endurance of 1/2 Percent Molybdenum Steel", _Proceedings of the Institution of Mechanical Engineers_, Vol. 84, p. 223, 1969-70.

9. Corwin, W. R., Brinkman, C. R., "Effects of Steam and Helium Envororments on the Elevated Temperature Subcritical Crack Growth of 2 1/4 Cr - 1 Mo Steel", _Proceedings of 2nd International Conference on Mechanical Behavior of Materials_, ASM, p. 1498, 1978.

10. _Nuclear Systems Materials Handbook_, Part I, Group 2, Section 2, Property Code 4102, "Air Side Corrosion", Revision June 27, 1974.

107

11. Langdon, R. L., *Calculation of the Oxide Growth Rate of 2 1/4 Cr - 1 Mo Steel in Air and the Subsequent Measurement of the Strain Required to Crack the Oxide*, MSME Thesis, Naval Postgraduate School, Monterey, Ca, September, 1980.

12. Griess, J. C., DeVan, J. H., and Maxwell, W. A., *Oxidation of Heated 2 1/4 Cr - 1 Mo Steel Tubing in Flowing Superheated Steam*, ORNL-5373, Oak Ridge National Laboratory, 1978.

13. Armitt, J., and others, *The Spalling of Steam Grown Oxide from Superheater and Reheater Tube Steels*, EPRI FP-686 TPS-655, Section 2, Electric Power Reasearch Institute, February, 1978.

14. Skelton, R. P., and Bucklow, J. I., "Cyclic Oxidation and Crack Growth during High Strain Fatigue of Low Alloy Steel", *Metal Science*, Vol. 12, p. 64, 1978.

15. Gordon, A. T., Bitsianes, G., and Joseph, T. L., "Thermal Expansion Cofficients for Iron and Its Oxides from X-ray Diffraction Measurements", *Transactions of the Metalurgical Society of AIME*, Vol. 233, pp. 1519-1524, August 1965.

16. McElroy, D. L., *Estimated Physical Properties of 2 1/4 Cr - 1 Mo Steel*, Oak Ridge National Laboratory, August 5, 1974.

17. Field, E. M. and others, "The Growth, Structure and Breakdown of Magnitite Films on Mild Steel", *Proceedings of the 2nd International Congress on Meterial Corrosion*, New York, p. 829, 1963.

18. Metcalfe, E., and Manning, M. I., *Mechanical Properties of Oxide Scales Formed on Austinetic Steels in Steam*, CEGB Report RD/L/N229/74, 1974.

19. Teranishi, H., and McEvily, A. J., "The Effects of Oxidation on Hold Time Fatigue Behavior of 2.25 Cr-1 Mo Steel", *Metallurgical Transactions A*, Vol. 10A, pp. 1806-1808, November, 1979.

20. Taylor, D., and Knott, "Fatigue Crack Propagation Behavior of Short Cracks: The Effect of Microstructure", *Fatigue of Engineering Materials and Structures*, Vol. 4, No. 2, pp. 147-155, 1981.

21. Skelton, R. F., "Crack Growth During High Strain Fatigue of 0.5 Cr-MO-V Steel at 825 K", *Materials Science and Engineering*, Vol. 32, pp. 211-219, 1978.

22. Skelton, R. P., and Challenger, K. D., "Fatigue Crack Growth in 2 1/4 Cr-1 Mo Steel at 525 6C, Parts I and II", accepted for publication in _Materials Science and Engineering_, 1984.

23. _Mechanical Properties Test Data for Structural Materials_, Progress Report for the Period ending April 30, 1975, Oak Ridge National Laboratory, ORNL-5105, pp. 8-10, June 1975.

24. Ellison, K. H., Unpublished Data, 1983

25. _MTS Model 410.31 Digital Function Generator_, 410.31 OF, Section 2, MTS Systems Corporation, 1975.

26. Hastie, W. A., _Design and Validation of an Apparatus for High Temperature Fatigue Testing in an Inert Environment_, MSME Thesis, Naval Postgraduate School, Monterey, 1981.

BIBLIOGRAPHY

Clark, C. L., _High Temperature Alloys_, Putman, 1953.

MTS Crerator's Manual Series 810, No. 976.01-30, MTS System Corporation, 1975.

MTS _Reference Manual, Vol I and II_, MTS Systems Corporation, 1982.

INITIAL DISTRIBUTION LIST

		No. Copies
1.	Defense Technical Information Center Cameron Station Alexandria, Virginia 22314	2
2.	Library, Code 0142 Naval Postgraduate School Monterey, California 93943	2
3.	Department Chairman, Code 69 Department of Mechanical Engineering Naval Postgraduate School Monterey, California 93943	1
4.	Professor K. D. Challenger Office of Naval Research, London Box 39 FPO, New York, New York 09510	7
5.	Associate Professor T. R. McNelly, Code 69Mc Department of Mechanical Engineering Naval Postgraduate School Monterey, California 93943	2
6	Adjunct Professor C.A. May, Code 69Mf Department of Mechanical Engineering Naval Postgraduate School Monterey, California 93943	1
7.	LCDR Orion P. Keifer 2250 Garland Lakewood, Colorado 80215	2

111

END

FILMED

4-85

DTIC